J. Fluid Mech. (1995), *vol.* 282, *pp.* 279–311

Three-dimensional structure of straight and curved plane wakes

By JAMES H. WEYGANDT[1]† AND RABINDRA D. MEHTA[1,2]

[1] Department of Aeronautics and Astronautics, JIAA, Stanford University, Stanford, CA 94305-4035, USA

[2] Fluid Mechanics Laboratory, NASA Ames Research Center, Moffett Field, CA 94035-1000, USA

(Received 24 January 1994 and in revised form 3 June 1994)

The formation and evolution of the three-dimensional structure of straight and mildly curved ($b/\bar{R} < 2\%$) flat plate wakes at relatively high Reynolds numbers ($Re_b = 28000$) have been studied through detailed measurements of the mean and fluctuating velocities. In both cases, the role of initial conditions was examined by generating wakes from untripped (laminar) and tripped (turbulent) initial boundary layers. The curved wake was affected by the angular momentum instability such that the inside half of the wake was unstable, whereas the outside half was stable. In both the straight and curved untripped wakes, large spanwise variations, in the form of 'pinches' and 'crests', were observed in the contours of mean velocity and Reynolds stresses. Well-organized, 'spatially stationary' streamwise vorticity was generated in the near-field region in the form of quadrupoles, to which the spanwise variations in the velocity contours were attributed. The presence of mean streamwise vorticity had a significant effect on the wake growth and defect decay rates, mainly by providing additional entrainment. In the straight wake, the mean streamwise vorticity decayed on both sides of the wake such that it had decayed completely by the far-field region. However, in the curved case, the mean streamwise vorticity on the unstable side decayed at a rate significantly lower than that on the stable side. Despite the decay of mean streamwise vorticity, the spanwise variations persisted into the far wake in both cases. The effects of curvature were also apparent in the Reynolds stress results which showed that the levels on the unstable side were increased significantly compared to those on the stable side, with the effect much stronger in the initially laminar wake. With the initial boundary layers tripped, spatially stationary streamwise vortex structures were not observed in either the straight or curved wakes and the velocity contours appeared nominally two-dimensional. This result further confirms the strong dependency of the three-dimensional structure of plane wakes on initial conditions.

1. Introduction

Wakes have many practical applications in various facets of aerodynamics and hydrodynamics. Wake flows are seen on turbomachinery blades, multi-element airfoils, and even on valves within a human heart. An understanding of the flow in the wake, in particular the three-dimensional structure, is essential to the prediction of performance of these important elements. This is because the pressure distributions over the rear part of the elements are affected by a complex interaction involving the boundary layers, wakes and the external potential flow field. The type of wake under

† Present address: Kawachi Millibioflight Project, Research Development Corporation of Japan, 4-7-6 Komaba Meguro, Tokyo 153, Japan.

study here is the streamlined-body wake, which is generated by bodies such as airfoils and flat plates.

For a fully turbulent wake, it is expected that at a large distance downstream the flow will become fully independent of the initial conditions and achieve an asymptotic, 'self-similar' state (Townsend 1976). The wake is said to have achieved a self-similar state when the mean and turbulence properties attain (universal) distributions which are independent of streamwise location when properly normalized by the characteristic length (half-width) and velocity (defect) scales. However, the behaviour of a turbulent wake in practice is not quite that simple. A recent study by Wygnanski, Champagne & Marasli (1986) showed that wakes generated by different bodies do not exhibit universal self-similar behaviour since the normalized velocity and length scales and distributions of the Reynolds stresses were found to be dependent on the geometry of the generating body. George (1989) suggested that the Reynolds stress profiles will differ by an amount proportional to the difference in wake growth rates. For a given generating body and initial conditions, though, universality in the self-similar behaviour is expected. Although there is a distinct lack of far-field data for the flat plate (turbulent) wake, for the few sets that exist a reasonable collapse of the mean and turbulence data has been observed (Weygandt & Mehta 1993).

A lot of studies have concentrated on wakes generated by bluff bodies, such as the circular cylinder. At least in terms of structure, there are many similarities between bluff-body wakes and those generated by streamlined bodies. It has long been known that the (initially laminar) wakes of two-dimensional bodies at moderate and high Reynolds numbers are marked by the formation of spanwise-coherent vortical structures of alternating sign forming the familiar Kármán vortex street (Roshko 1954; Townsend 1956; Taneda 1959; Morkovin 1964). It was realized relatively early on that on additional secondary (three-dimensional) structure also evolves in the plane wake (Grant 1958; Gerrard 1966). Since then detailed measurements have revealed that the three-dimensional structure is composed of a distortion of the spanwise structures and the generation of streamwise vortices (Wei & Smith 1986; Hayakawa & Hussain 1989; Williamson 1992).

The formation of streamwise vorticity in wakes is expected to be similar to that in mixing layers, where it has been widely studied (see Bell & Mehta 1992, for a review). Rogers & Moser (1992) have shown that the three-dimensional instability responsible for the generation of the streamwise vortices in mixing layers is governed by two interacting mechanisms. One mechanism leads to the bending of the spanwise structures while the other leads to the formation of 'rib' vortices in the braids. These features (braids, spanwise structures) are also present in the wake and so the same instabilities should be responsible for the formation of the three-dimensionality observed in wakes. The subsequent evolution of the three-dimensionality is also found to be similar in the two shear flows (Meiburg & Lasheras 1988).

Meiburg & Lasheras (1988) investigated the structure of a perturbed splitter plate wake through inviscid vortex simulations and low Reynolds number flow visualization experiments and found that the redistribution, reorientation, and stretching of vorticity produced counter-rotating pairs of streamwise vortices which were superimposed onto the spanwise vortices. These streamwise vortices were in the form of lambda-shaped structures and resided in the braid regions connecting adjacent (opposite-signed) spanwise vortices. Subsequent interaction of the streamwise and spanwise structures led to the formation of closed vortex loops. In terms of the streamwise development, Breidenthal (1980) examined the structure in both a wake and a mixing layer formed downstream of a splitter plate with a spanwise-varying trailing edge and found that the

wake, unlike the mixing layer, remembered the initial perturbation and its distorted structure persisted into the far-field region. Streamwise vorticity has also been observed in direct numerical simulations of plane (transitional) wakes (Buell & Mansour 1989; Chen, Cantwell & Mansour 1990; Maekawa, Moser & Mansour 1993). The simulation results showed that the morphology of the streamwise vorticity was strongly dependent on the details of the initial (three-dimensional) disturbance field.

It is well known that even mild streamwise curvature has a profound effect on turbulent shear flows (Bradshaw 1973). An inviscid instability occurs in a shear flow in which the angular momentum decreases away from the centre of curvature, thus making the boundary layer on a concave surface unstable while that on a convex surface is stable. The curved wake is particularly interesting since it contains both destabilizing (inner-half) and stabilizing (outer-half) regions. Most past experimental curved wake studies have concentrated on cylinder and airfoil wakes with the data always composed of single profile measurements made along the model centreline (Koyama 1983; Savill 1983; Nakayama 1987; Ramjee, Tulapurkara & Rajasekar 1988; Ramjee & Neelakandan 1989, 1990). The curvature ratio ($b/\bar{R}$) in all these studies was typically higher (2–15%) than that investigated in the present experiments ($b/\bar{R} < 2\%$). Although the results of these previous investigations do not totally agree on the effects of curvature on the Reynolds normal stresses, they are consistent on the sensitivity of the Reynolds shear stress ($\overline{u'v'}$) – the magnitude of the peak shear stress is increased on the unstable side compared to the straight case, while that on the stable side is decreased.

Ramjee *et al.* (1988) and Ramjee & Neelakandan (1989, 1990) examined the wakes of a rectangular cylinder and an airfoil developing in a longitudinally curved duct and found that the mean velocity profiles of the wakes were not symmetric about the centreline. The unstable side contribution to the half-width was greater than that of the stable side. They also reported that the wake defect was greater in the curved duct than in the straight duct, although no explanation was offered for this phenomenon.

While some work has already been conducted on the three-dimensional structure of straight wakes, and on the effects of streamwise curvature, many issues still remain unresolved. The formation and development of the streamwise vortical structures are not yet fully understood, particularly at relatively high Reynolds numbers. Previous studies of the streamwise vorticity in wakes have consisted mainly of qualitative flow visualization studies and direct numerical simulations, both conducted at relatively low Reynolds numbers and restricted to the near-field region. The effects of streamwise curvature on the three-dimensional structure of the wake have not been investigated at all. Accordingly, in the present study, the three-dimensional structure of straight and curved plane wakes are investigated quantitatively through detailed time-averaged measurements. In particular, results showing the initial distribution, reorganization and evolution of the streamwise vortical structures are presented. Their effects on the near- and far-field development of both wakes are studied and the issue of self-similarity is addressed. In both the straight and curved cases, the effects of changing the state of the initial boundary layers from laminar to turbulent are also discussed. Some of the more important results are presented in this paper; full details of this investigation are given in Weygandt & Mehta (1993).

2. Experimental apparatus and techniques

The experiments were performed in a shear layer wind tunnel (figure 1) which was designed so that different test-section configurations could be easily attached

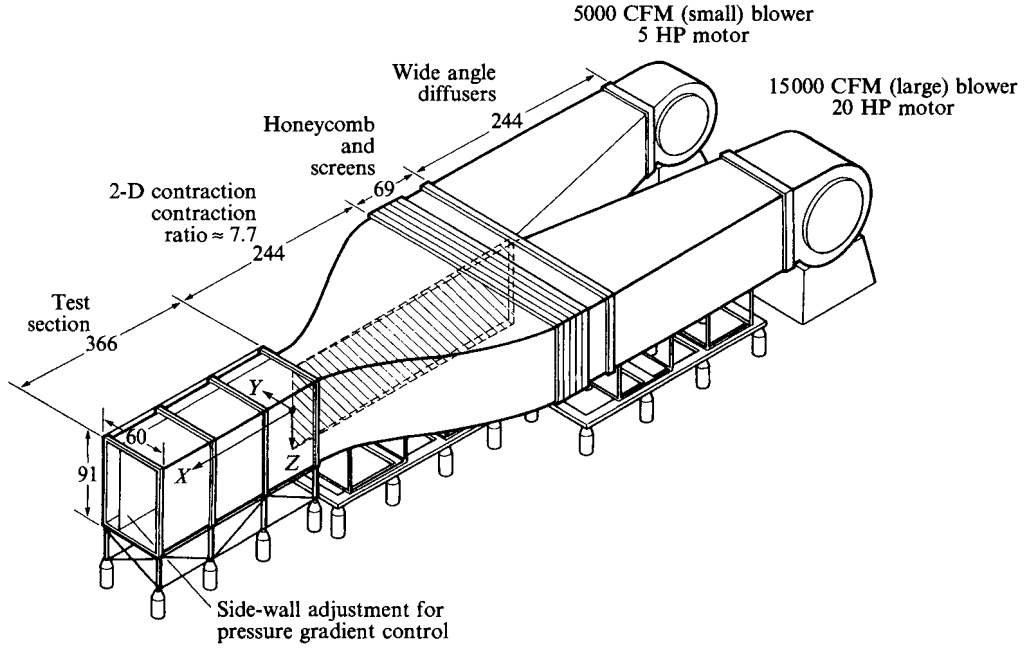

FIGURE 1. Schematic of shear layer wind tunnel. All dimensions in cm.

downstream of the contraction. The wind tunnel consists of two separate legs, each independently driven by a centrifugal blower. Upon exiting the blowers, the air is passed through individual wide-angle diffusers, flow conditioning elements, and two separate, but identical, 8:1 two-dimensional contraction sections. The two flows merge in the test section, downstream of the sharp trailing edge of a long, slowly tapering splitter plate with an included angle of 1°.

The base tunnel configuration consists of a straight test section which is 36 cm wide in the cross-stream (Y) direction, 91 cm high in the spanwise (Z) direction, and 3.7 m long in the streamwise (X) direction. The velocities are defined such that u, v and w are the instantaneous velocities in the X-, Y- and Z-directions, respectively. The sidewall on the small blower side is movable and slotted, allowing probe access. For the present experiments, this wall was adjusted to give a nominally zero pressure gradient – streamwise variation in free-stream velocity was less than 1%. For the curved wake experiments, a curved test section (figure 2) was attached to the contraction exit. The curved test section, measuring 3.7 m along the centreline arc, has a fixed mean radius ($\bar{R}$) of 305 cm, giving a maximum $b/\bar{R}$ (where b is the wake half-width) of less than 2%. The constant curvature is applied immediately from the trailing edge of the splitter plate and extends up to the end of the test section. As in the straight test section, one sidewall is slotted and movable and it was also adjusted to give a nominally zero streamwise pressure gradient.

In the present experiments, the two sides of the wind tunnel were run at free-stream velocities (U_e) in the test section of 9 m s^{-1}. In the curved case, the angular momentum (UR, where R is the local radius of curvature), and not the velocity, is constant in the potential flow. Therefore, UR was monitored on the two sides to ensure that a wake (and not a mixing layer) was developing in the test section. In both cases, the tunnel velocities were held constant to within 1% during a typical run lasting 2–4 h. At these operating conditions, the measured streamwise turbulence intensity level (u'/U_e) was

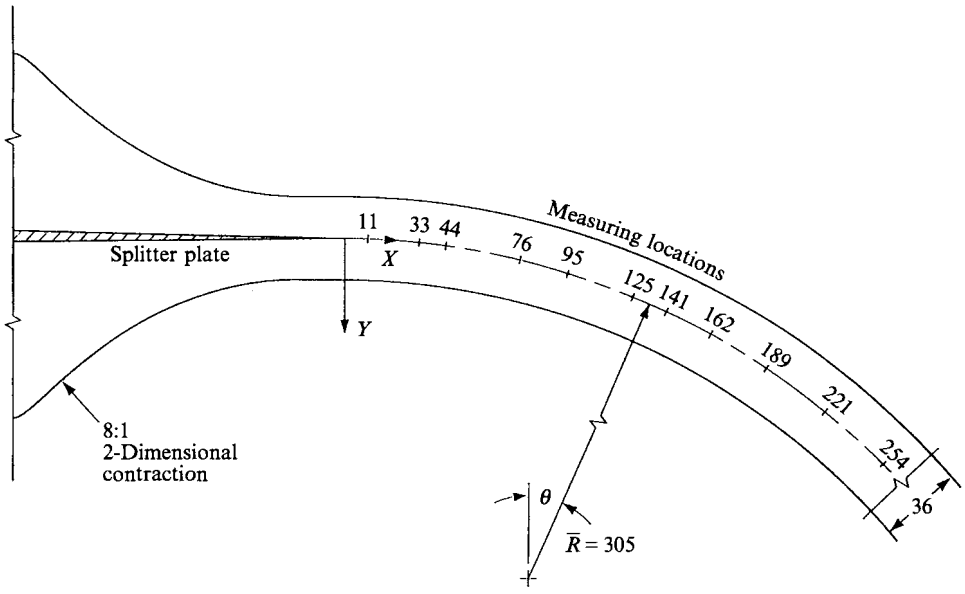

FIGURE 2. Schematic of curved test section. All dimensions in cm.

about 0.15% and the transverse levels (v'/U_e and w'/U_e) were about 0.05%. The mean core flow in the test section was found to be uniform to within 0.5% and the cross-flow angles were less than 0.25°. Further details of the wind tunnel design and performance characteristics are given in Bell & Mehta (1989).

In both the straight and curved wakes, two initial conditions were studied, namely untripped (laminar) and tripped (turbulent) boundary layers at the splitter plate trailing edge. In the tripped cases, the boundary layers were perturbed by gluing a 1.5 mm diameter round wire to each side of the splitter plate at a location 18 cm upstream of the trailing edge. The boundary layer properties for both initial conditions are given in table 1. The boundary layer properties were averaged over five spanwise locations, although they varied by less than 2%, indicating adequate two-dimensionality.

Measurements were obtained using a rotable cross-wire probe (Dantec Model 55P51) operated by Dantec 55M10 anemometers. The probe consisted of 5 μm diameter platinum-plated tungsten sensing elements approximately 1 mm in length and separated by approximately 1 mm. The signals were filtered (low-pass at 30 kHz), DC offset, and amplified by a factor of 10 before being fed into a Tustin (Model 110-9C) fast sample-and-hold A/D converter with 15 bit resolution and onto a Micro Vax II computer system. The probe was calibrated statically in the potential core of the flow (between the wake and the wall boundary layer) assuming a 'cosine law' response to yaw, with the effective angle determined by calibration. The wind tunnel reference velocity (used for normalizing the data) and flow temperature (used for correcting the cross-wire data) were also acquired through the A/D system. Individual statistics were calculated by averaging over 5000 samples of cross-wire data obtained at a rate of 1500 Hz.

Data were obtained in cross-sectional (Y, Z) planes at 10 streamwise locations in the straight wake and at 11 locations in the curved wake with the cross-wire oriented in two planes (uv and uw). This yielded all three components of mean velocity, five of the six Reynolds stresses ($\overline{v'w'}$ was not measured) and selected higher-order products. For the curved cases, the measurements were made along the local radius, with the probe tip

Condition	U_e (m s^{-1})	δ_{99} (cm)	θ (cm)	Re_θ $U_e\theta/\nu$	H δ^*/θ
Large untripped	9.0	0.44	0.055	322	2.61
Small untripped	9.0	0.44	0.061	362	2.24
Large tripped	9.0	0.95	0.099	596	1.49
Small tripped	9.0	0.98	0.119	700	1.32

TABLE 1. Initial boundary layer properties

Streamwise location X (cm)	Cross-stream range Y (cm)	Spanwise range Z (cm)	Grid spacing (cm)	Grid size	Number of points per plane
7.8	−1.2–1.2	−2.8–2.8	0.10	25 × 57	1425
16.7	−1.5–1.5	−4.5–4.5	0.15	21 × 61	1281
27.0	−2.5–2.5	−8.0–8.0	0.25	21 × 65	1365
57.3	−4.0–4.0	−14.0–14.0	0.40	21 × 71	1491
77.6	−4.0–4.0	−14.0–14.0	0.40	21 × 71	1491
108.1	−5.0–5.0	−17.5–17.5	0.50	21 × 71	1491
128.4	−5.0–5.0	−17.5–17.5	0.50	21 × 71	1491
158.4	−6.6–6.6	−18.0–18.0	0.60	23 × 61	1403
189.4	−7.7–7.7	−20.3–20.3	0.70	23 × 59	1357
250.3	−8.8–8.8	−20.0–20.0	0.80	23 × 51	1173

TABLE 2. Cross-wire measurement locations: straight untripped wake

Streamwise location X (cm)	Cross-stream range Y (cm)	Spanwise range Z (cm)	Grid spacing (cm)	Grid size	Number of points per plane
11.4	−1.8–1.2	−4.5–4.5	0.15	21 × 61	1281
33.0	−2.6–1.4	−7.0–7.0	0.20	21 × 71	1491
43.8	−3.0–2.0	−8.0–8.0	0.25	21 × 71	1365
76.1	−4.0–3.7	−12.3–12.3	0.35	23 × 71	1633
95.0	−4.4–4.4	−14.0–14.0	0.40	23 × 71	1633
124.7	−5.0–5.0	−17.5–17.5	0.50	21 × 71	1491
140.9	−6.0–6.0	−19.2–19.2	0.60	21 × 65	1365
162.4	−6.6–6.6	−20.4–20.4	0.60	23 × 69	1587
188.9	−7.5–7.5	−21.8–20.3	0.75	21 × 57	1197
221.3	−8.0–8.0	−22.4–20.8	0.80	21 × 55	1155
253.6	−8.8–8.8	−22.4–20.8	0.80	23 × 55	1265

TABLE 3. Cross-wire measurement locations: curved untripped wake

aligned with the local streamline. The location and size for the untripped straight and curved data planes are given in tables 2 and 3, respectively – those for the tripped cases were very similar. In order to study the streamwise development of the wake, its global properties, such as the defect and half-width, were evaluated through a spanwise averaging technique. Since full details of this technique, including its implications, are given in Bell, Plesniak & Mehta (1992), only a brief description is included here. The spanwise-averaged quantities were evaluated by dividing the measurements obtained on the cross-plane grid into individual Y-profiles or 'slices' through the wake. The wake properties for each slice were computed in the traditional manner and then algebraically averaged over all spanwise positions, giving a single value for each quantity. In effect, depending on the streamwise location, the properties were averaged

over 50 to 70 individiual spanwise profiles covering a spanwise extent of approximately ten wake half-widths.

An error analysis, based on calibration accuracy and repeatability of measurements, indicates that mean streamwise velocity measurements with the cross-wire are accurate to within 3%, while mean cross-stream velocities are accurate to within 10%. Reynolds normal stress measurements are accurate to within 6%, and shear stresses are accurate to within 15–20%. The measurements were corrected for mean streamwise velocity gradient ($\partial U/\partial Y$ and $\partial U/\partial Z$) effects – details of the correction scheme are given in Weygandt & Mehta (1993). The streamwise component of mean vorticity (Ω_x) was computed using a central difference numerical differentiation of the V and W measurements. The overall circulation (Γ) was determined from the surface integral of the streamwise vorticity field over the cross-flow plane, with vorticity levels less than 20% of the maximum value being set to zero in order to provide immunity from 'noise'. The integration was applied across a 'box' on the measured grid that fully encompassed each identified vortex (that containing at least two closed vorticity contours with the spacing of the contour levels chosen to equal 10% of $(\Omega_x)_{max}$). The mean streamwise vorticity measurements were repeatable to within about 20% while the circulation measurements were repeatable to within about 25%.

3. Results and discussion

The data presented in this paper are normalized using two velocity scales. The 'raw' data are normalized by the free-stream (tunnel reference) velocity, U_e, which for the curved case is defined as $U_e = (U_r R_r)/\bar{R}$, where U_r is the reference tunnel velocity measured at a radial location, R_r, which corresponds to the calibration location ($Y = 8.9$ cm). The calibration location was chosen to lie in the potential core, halfway between the wake centreline and the sidewall. Some of the presented data are normalized by the wake velocity defect, U_0, defined as $U_0 = U_e - U_{min}$, where U_{min} is the minimum velocity in the wake. For the curved wake, the velocity defect is defined as $U_0 = [(RU)_e - (UR)_{min}]/\bar{R}$. The wake lengthscale, the half-width (b), is defined as the distance between points in the mean velocity profile where the velocity is equivalent to $U_e - U_0/2$.

The contour plots for the untripped wakes presented below were constructed from cross-sectional planes of data. Details of the cross-sectional grids on which the measurements were made are given in table 2 for the straight untripped wake and in table 3 for the curved untripped wake for all streamwise locations so that the acquired spatial resolution may be determined. In general, on a given contour plot, the grid spacing is equivalent to the diameter of the smallest closed contour.

3.1. *Mean velocity and Reynolds stresses*

Contours of the mean streamwise velocity (U/U_e) measured at the first and last stations for the straight and curved untripped cases are presented in figures 3 and 4, respectively. The locations for the straight and curved cases are not exactly the same, but they are close enough for the purposes of qualitative comparison. Note that for the curved wake the positive-Y side represents the unstable side while the negative-Y side is stable.

In the near-field region (figures 3*a* and 4*a*), both cases exhibit a distinctive spanwise distortion in the form of a 'pinching' and 'cresting'. Qualitatively, the quasi-periodic variation is more severe in the curved wake. Regions of minimum velocity or maximum defect appear along the wake span at approximately 2–4 cm intervals. The spanwise

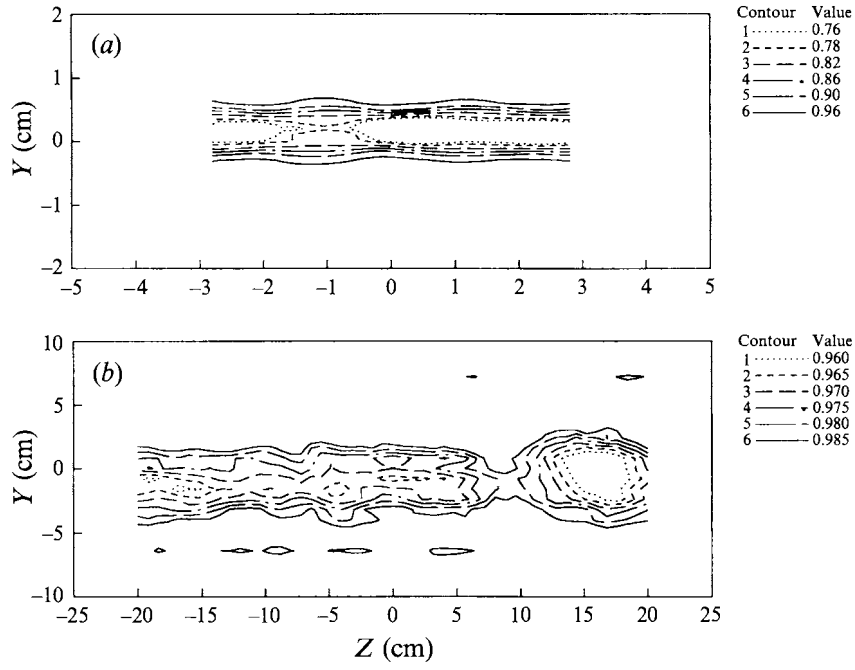

FIGURE 3. Mean streamwise velocity (U/U_e) contours for the straight untripped case: (*a*) $X = 8$ cm; (*b*) $X = 250$ cm.

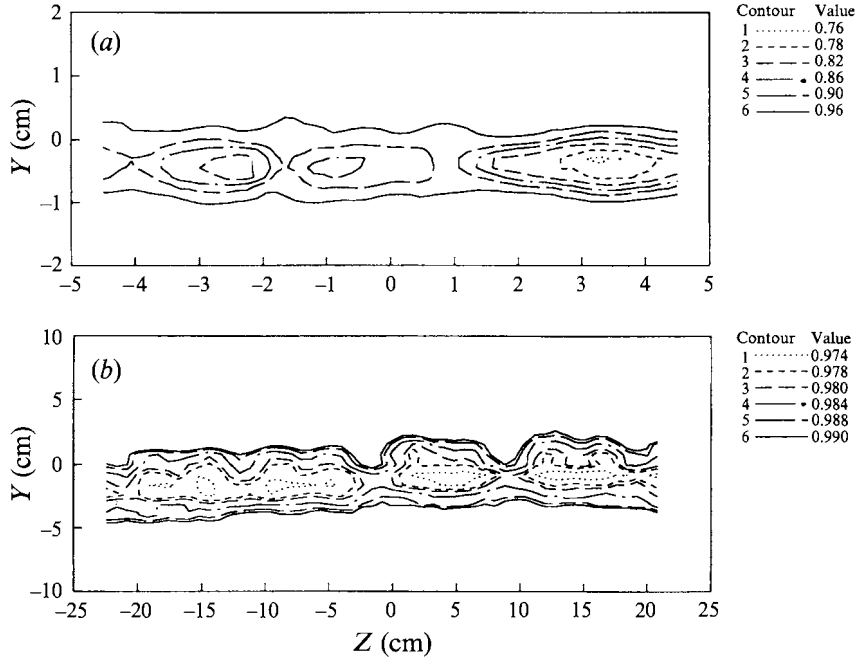

FIGURE 4. Mean streamwise velocity (U/U_e) contours for the curved untripped wake: (*a*) $X = 11$ cm; (*b*) $X = 254$ cm.

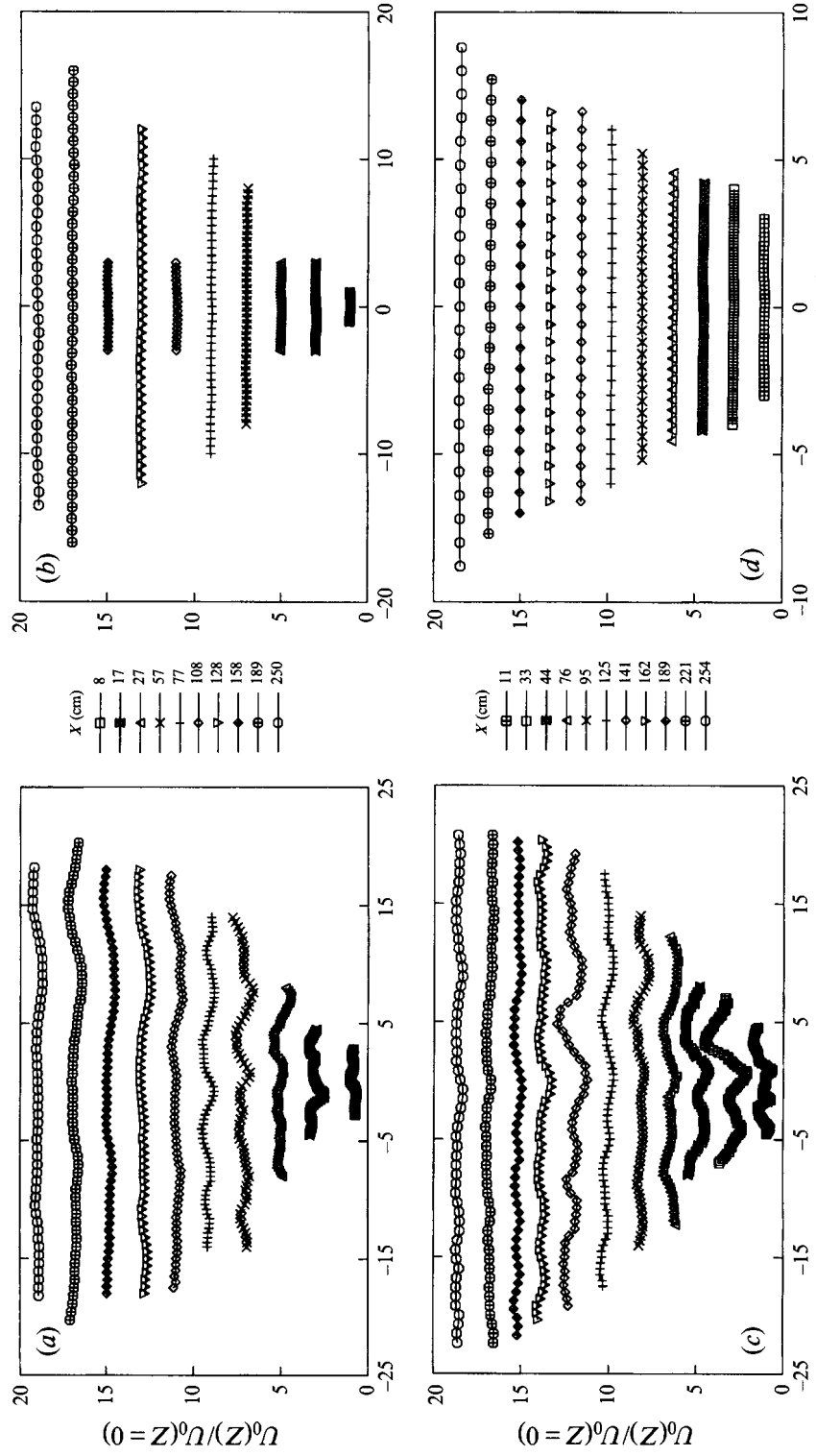

FIGURE 5. Spanwise variation of wake defect (U_0): (*a*) straight untripped wake; (*b*) straight tripped wake; (*c*) curved untripped wake; (*d*) curved tripped wake.

variation in both the straight and curved untripped wakes is seen to persist into the far-field region (figures 3*b* and 4*b*). The regions of maximum velocity defect are now spaced at about 10 cm in both cases. Once again, the curved case appears slightly more distorted than the straight case, with the distortion more prominent on the unstable (positive-Y) side. The difference in the level of distortion between the two cases is related to the strength of the streamwise vortices, as further discussed below in §3.2. A detailed comparison of the streamwise development of the mean velocity contours for the two cases in the far-field region (Weygandt & Mehta 1993) showed some interesting differences. The distortions and locations of the maximum defect regions in the straight case were 'trackable' from one streamwise station to the next. However, in the curved case, the distorted contours and locations of the maximum defect regions change with streamwise distance and thus were not readily trackable. The velocity contours for the two (straight and curved) tripped cases are not presented here since they were found to be nominally straight and parallel throughout the wake development, comparable to those expected for a two-dimensional wake.

The streamwise development of the spanwise distributions of the wake defect and half-width (normalized by the centreline value at $Z = 0$ cm) for the four cases are compared in figures 5 and 6, respectively. Note that the profiles are staggered vertically in order to improve readability. Both the straight and curved untripped wakes exhibit large spanwise variations in the defect and half-width in the near-field region. Although the magnitude of the spanwise variation decays with streamwise distance, the variation clearly persists into the far wake in both untripped cases. In the near wake, the straight case has standard deviations in defect and half-width of approximately 10–20%, compared to 20–30% for the curved case, showing that the curvature begins to affect the wake three-dimensionality almost immediately. Further downstream, however, the standard deviation in both the curved and straight cases is about the same (20%). Also, the wavelength of the spanwise variation of both quantities increases with streamwise distance in both cases. Both the straight and curved tripped wakes show little spanwise variation in defect and half-width throughout their streamwise development, further confirming their two-dimensionality in the mean sense. The magnitudes of the maximum variation in defect and half-width in the far wake ($X \approx 250$ cm) is about 6% for the tripped cases compared to the 20% for the untripped cases.

The large spanwise distortions observed in the mean velocity contours for the untripped cases were also apparent in the Reynolds stress contours. As with the mean velocity contours, the Reynolds stress contours for both the tripped cases did not exhibit any significant spanwise variations. Contours of the primary shear stress ($\overline{u'v'}/U_e^2$) measured at the first and last stations for the straight and curved untripped cases are given in figures 7 and 8, respectively; the contours of all the measured Reynolds stress components for all the cases are given in Weygandt & Mehta (1993). In the straight untripped wake at $X = 8$ cm (figure 7*a*), the familiar antisymmetric distribution is apparent, with peaks of equal magnitude, but opposite sign, on the two sides of the wake. The shear stress contours depict the crested/pinched effect seen in the mean velocity contours and the peaks on both sides of the wake appear almost uniformly along the span. However, the peaks became more localized with increasing downstream distance and their positions were found to be correlated with the peaks in the normal stresses and dips in the mean velocity. The spanwise variation and local peaks are seen to persist into the far-field region and the maximum positive and negative levels are still about equal (figure 7*b*). The curved untripped wake $\overline{u'v'}$ contours appear more complex than those of the straight wakes even at the first station (figure 8*a*). Both positive and negative shear stress peaks are evident on the two sides

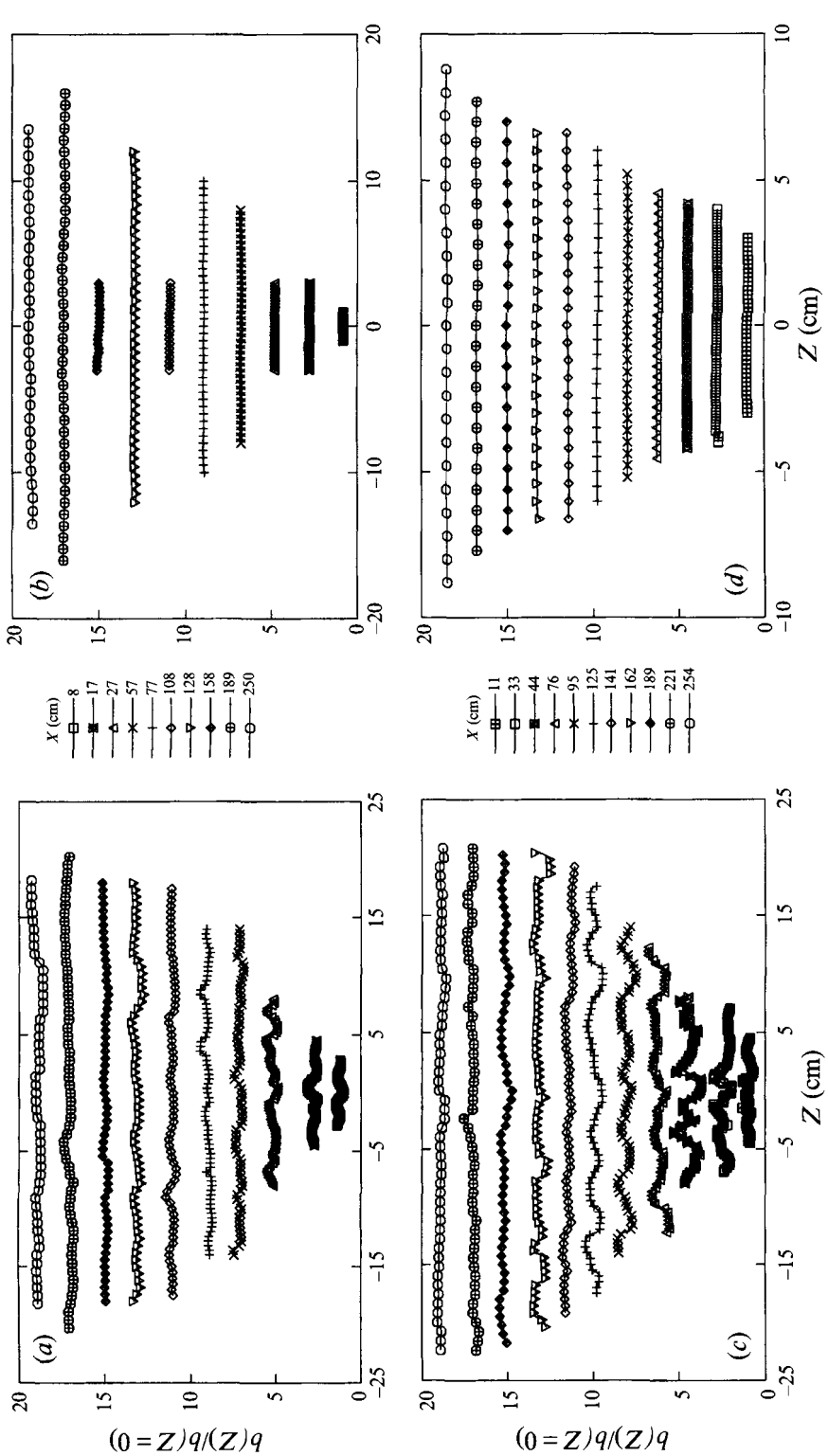

FIGURE 6. Spanwise variation of wake half-width (b): (*a*) straight untripped wake; (*b*) straight tripped wake; (*c*) curved untripped wake; (*d*) curved tripped wake.

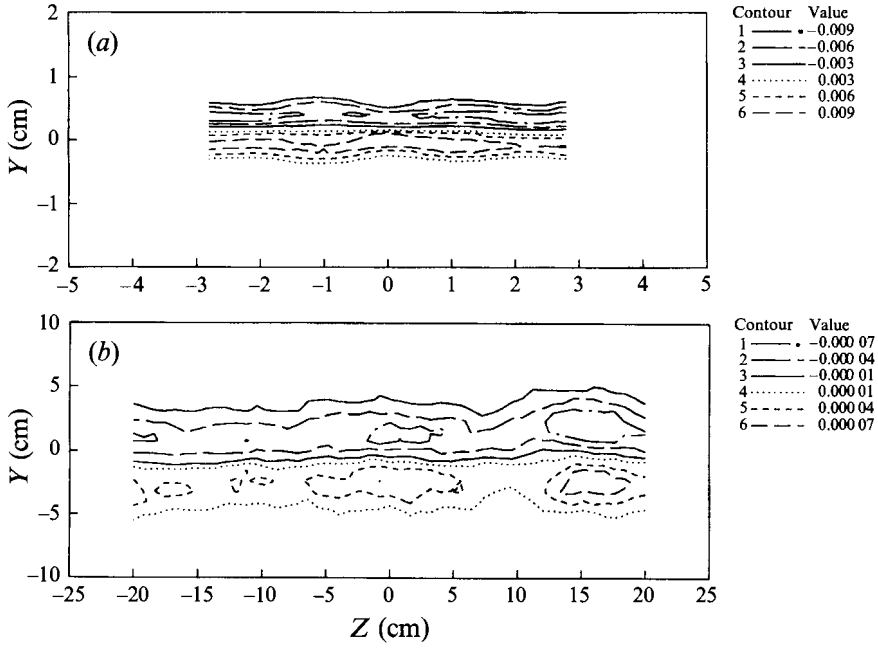

FIGURE 7. Primary shear stress ($\overline{u'v'}/U_e^2$) contours for the straight untripped wake: (*a*) $X = 8$ cm; (*b*) $X = 250$ cm.

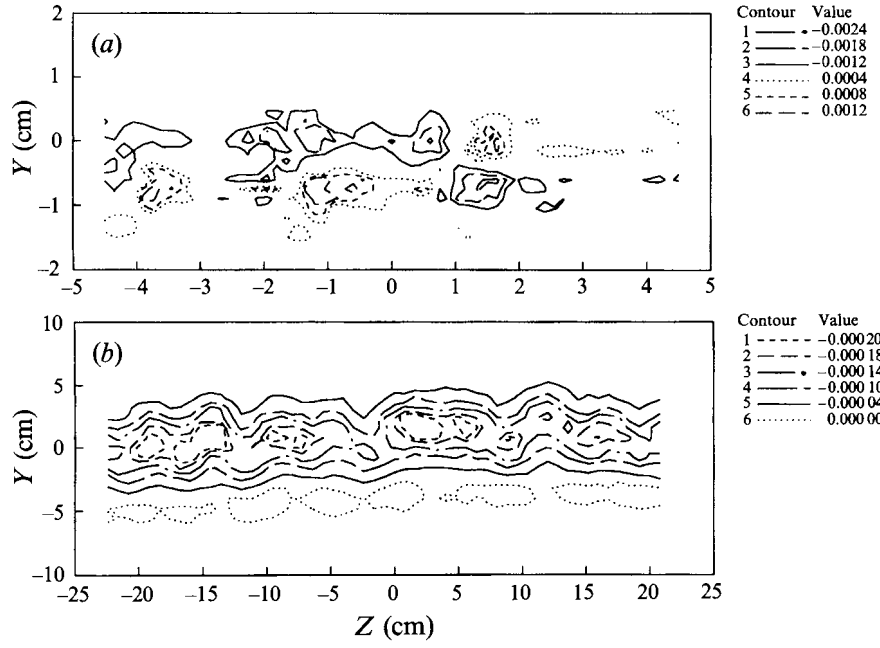

FIGURE 8. Primary shear stress ($\overline{u'v'}/U_e^2$) contours for the curved untripped wake: (*a*) $X = 11$ cm; (*b*) $X = 254$ cm.

of the wake. The effects of curvature can already be seen at this near-field station, with the magnitude of negative shear stress on the unstable side of the wake approximately twice the magnitude of positive shear stress on the stable side. The asymmetry in levels was found to grow with downstream distance such that by $X = 254$ cm, the shear stress

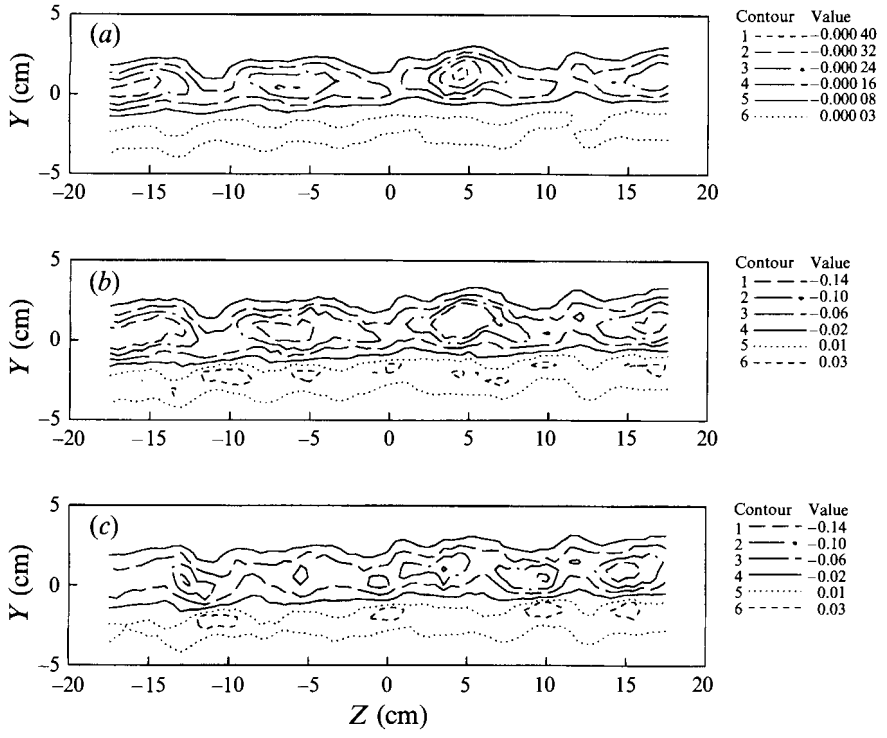

FIGURE 9. Primary shear stress contours with different normalizations for the curved untripped wake at $X = 125$ cm: (*a*) normalized by free-stream velocity; (*b*) normalized by spanwise-averaged defect; (*c*) normalized by local defect.

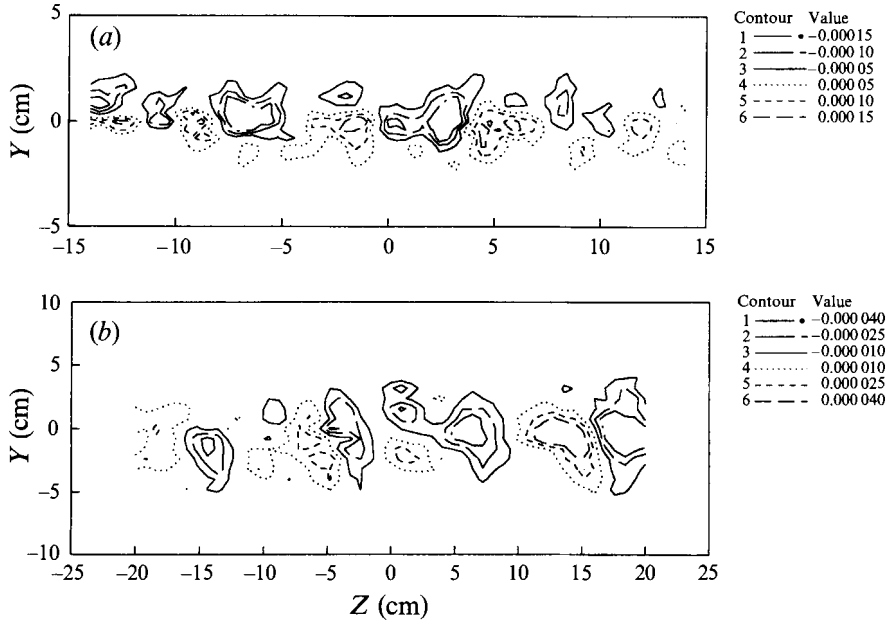

FIGURE 10. Secondary shear stress ($\overline{u'w'}/U_e^2$) contours for the straight untripped wake: (*a*) $X = 77$ cm; (*b*) $X = 250$ cm.

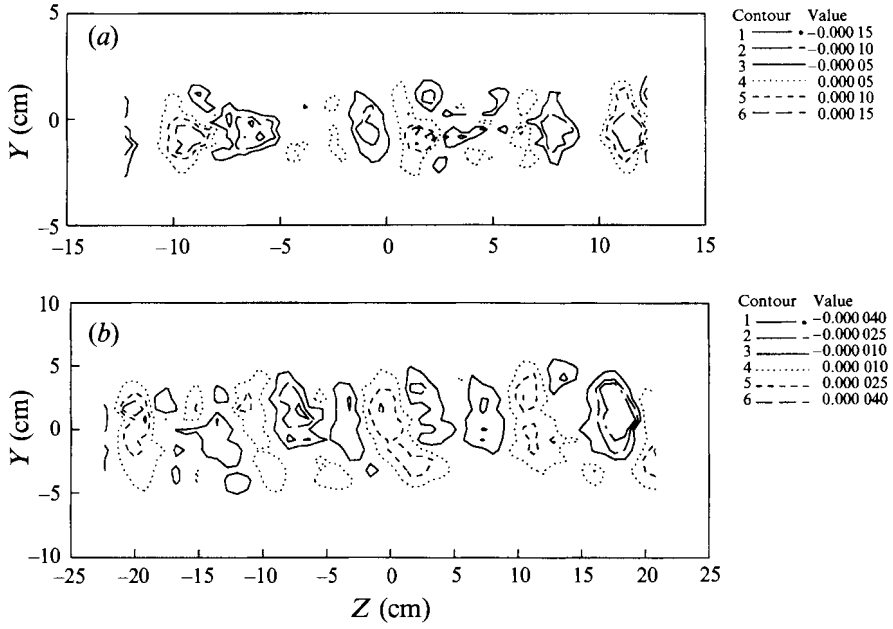

FIGURE 11. Secondary shear stress $(\overline{u'w'}/U_e^2)$ contours for the curved untripped wake: (*a*) $X = 76$ cm; (*b*) $X = 254$ cm.

level on the unstable side is an order of magnitude higher than the level on the stable side (figure 8*b*). The negative shear stress peaks were found to be fairly well correlated in position with peaks in the turbulent kinetic energy contours and dips in those of mean velocity.

The Reynolds stress contours presented above are normalized by the free-stream velocity, U_e. As discussed above in §1, a more appropriate velocity scale for the wake is the defect, U_0. Of course, normalizing by a spanwise-averaged defect is not going to affect the (qualitative) distribution of the Reynolds stress contours. However, normalizing by a 'local' defect should be more revealing since the positions of local peaks in the Reynolds stress contours were seen to correspond to dips (regions of maximum defect) in the mean streamwise velocity contours.

Figure 9(*a–c*) shows a comparison of the $\overline{u'v'}$ contours for the curved untripped wake at $X = 125$ cm normalized by free-stream velocity, spanwise-averaged defect, and 'local' velocity defect. All three contour plots exhibit similar spanwise variations, at least qualitatively. In particular, normalizing by the local defect does not wash out the spanwise variation in the Reynolds stress contours, but it does shift the peak locations such that they now appear in regions of relatively low original stress. This implies that the defect in these regions is lower than would be expected for a given stress level, thus resulting in regions of high stress in the local defect normalized plot. The regions of high defect and high local Reynolds stresses are in phase, but the relative magnitude of the defect is such that the spanwise variation is not washed-out by this normalization. In essence, what these results really imply is that the production of $\overline{u'v'}$ is no longer solely determined by $\partial U/\partial Y$, as in two-dimensional shear flows. Production terms with cross-stream (Y) and spanwise (Z) gradients of the secondary mean velocities (V and W) would also be expected to contribute, as shown below in §3.5. So the three-dimensionality of the wake is more complicated than a simple superposition of individual profiles of differing wake parameters.

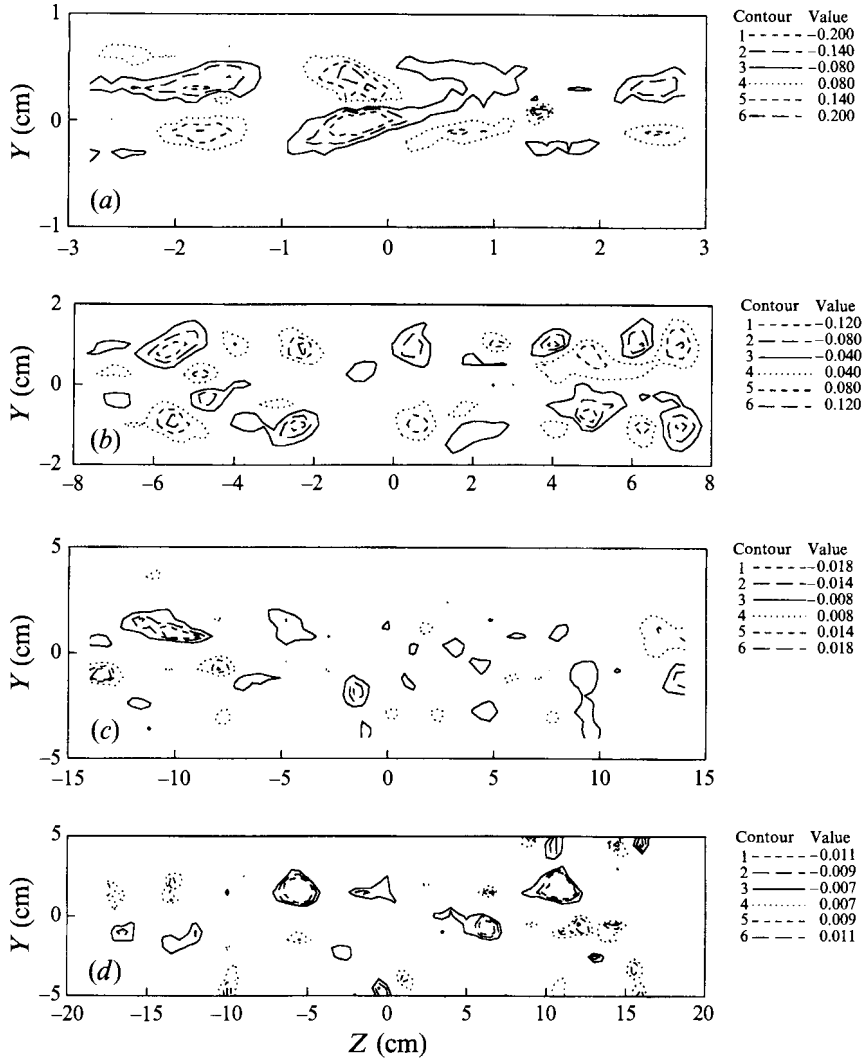

FIGURE 12. Mean streamwise vorticity (Ω_x/U_e, cm^{-1}) contours for the straight untripped wake: (*a*) $X = 8$ cm; (*b*) $X = 27$ cm; (*c*) $X = 77$ cm; (*d*) $X = 108$ cm.

With both untripped wakes exhibiting a strong three-dimensional structure, it is not surprising to see that significant levels of the secondary shear stress ($\overline{u'w'}/U_e^2$) are generated (figures 10 and 11). Starting at $X \approx 76$ cm, $\overline{u'w'}$ appears in a single row of alternating-signed 'islands' in both cases (figures 10*a* and 11*a*) and this form of the $\overline{u'w'}$ distribution persists right up to the last measurement station (figures 10*b* and 11*b*). This is very similar to the distribution of $\overline{u'w'}$ observed in straight (Bell & Mehta 1992) and curved (Plesniak, Mehta & Johnston 1994) mixing layers. At a given streamwise station, the peak levels of $\overline{u'w'}$ are comparable to those of the primary shear stress ($\overline{u'v'}$). On examining the transport equation for $\overline{u'w'}$ (equation (3.5)), it was found that the dominant production term in this region is $\overline{w'^2}\,\partial U/\partial Z$ (Weygandt & Mehta 1993). The pinching and cresting in the mean velocity contours (figures 3 and 4), produce a spanwise-varying $\partial U/\partial Z$ on both sides (positive- and negative-Y) of the wake. On both sides, the variation is in the form of alternating positive and negative peaks, but in phase such that a given spanwise location, the $\partial U/\partial Z$ peaks carry the same sign on the

two sides. With $\overline{w'^2}$ being relatively high on either side of the wake centreline, a single row of alternating-signed $\overline{u'w'}$ is thus generated. Since the spanwise variation in mean velocity, and hence $\partial U/\partial Z$, persists into the far-field region of the untripped wakes, so does the production of $\overline{u'w'}$.

3.2. *Mean streamwise vorticity*

As shown in the mean velocity and shear stress contours, the untripped wakes show a complex (three-dimensional) behaviour, which is attributable to the presence of streamwise vorticity. The role of the streamwise vorticity can be first investigated by examining the contour plots of mean streamwise vorticity (Ω_x/U_e). The contours, measured at four representative stations for the straight and curved untripped cases, are presented in figures 12 and 13, respectively.

In the near-field region for the straight case ($X = 8$ cm), two rows of alternating-sign vortices are evident on either side of the wake centreline ($Y = 0$), as shown in figure 12(*a*), similar to the structures reported by Lasheras & Meiburg (1990). The mean vorticity is arranged in groups or quadrupoles of four vortices consisting of two vortices on each side of the wake, with like-sign vortices diagonally opposite one another, such as the group at $Z \sim -1$ cm. The quadrupole positions coincide approximately with the crest/pinch locations in the mean velocity contours (figure 3*a*), which is anticipated because it is the two sets of counter-rotating vortices which induce the cross-flow momentum transport which produces the pinching and cresting in the velocity contours. The common flow between adjacent vortices produces either an inward (towards the wake centreline) or outward normal velocity (V) component, depending on the signs and orientation of the vortices. At this first station, the peak levels of mean streamwise vorticity on the two sides of the wake centreline are comparable and they are equivalent to about 20% of the estimated spanwise vorticity at this location. This uniform trend, and the distribution of the vorticity in quadrupoles, continues through to $X = 27$ cm (figure 12*b*), although the peak vorticity levels have decayed. Further downstream at $X = 77$ cm (figure 12*c*), the quadrupoles are still present, although they are becoming harder to discern since the peak vorticity levels continue to decrease with increasing streamwise distance. The spacing between the vortical structures has also increased. At $X = 108$ cm (figure 12*d*), the quadrupoles are even weaker and they continue to decay further downstream (symmetrically about the wake centreline) such that the vorticity levels become comparable to the background 'noise'.

It is interesting that the crested/pinched effect in the mean velocity and Reynolds stress contours persists into the far-field region (figures 3 and 4), although the quadrupoles of mean streamwise vorticity which produced these distortions have decayed. This provides further evidence, and confirms the earlier observations of Breidenthal (1980), of how slowly spanwise perturbations decay in the straight wake. As a result, the strong correlation between the mean streamwise vorticity (Ω_x) and the secondary shear stress ($\overline{u'w'}$), previously observed in mixing layers (Bell & Mehta 1992; Plesniak *et al.* 1994), does not exist in plane wakes.

The mean streamwise vorticity contours at the first station ($X = 11$ cm) for the curved untripped case (figure 13*a*) also exhibit a distribution consisting of quadrupoles with their locations similar to those in the straight case, although the vortices here are slightly larger and spaced further apart – note that this first station in the curved case is further downstream (by 3 cm) than that in the straight case. This implies that the formation process of the streamwise vorticity is not affected significantly by curvature and that the instability in both cases triggers-off the same incoming spatial

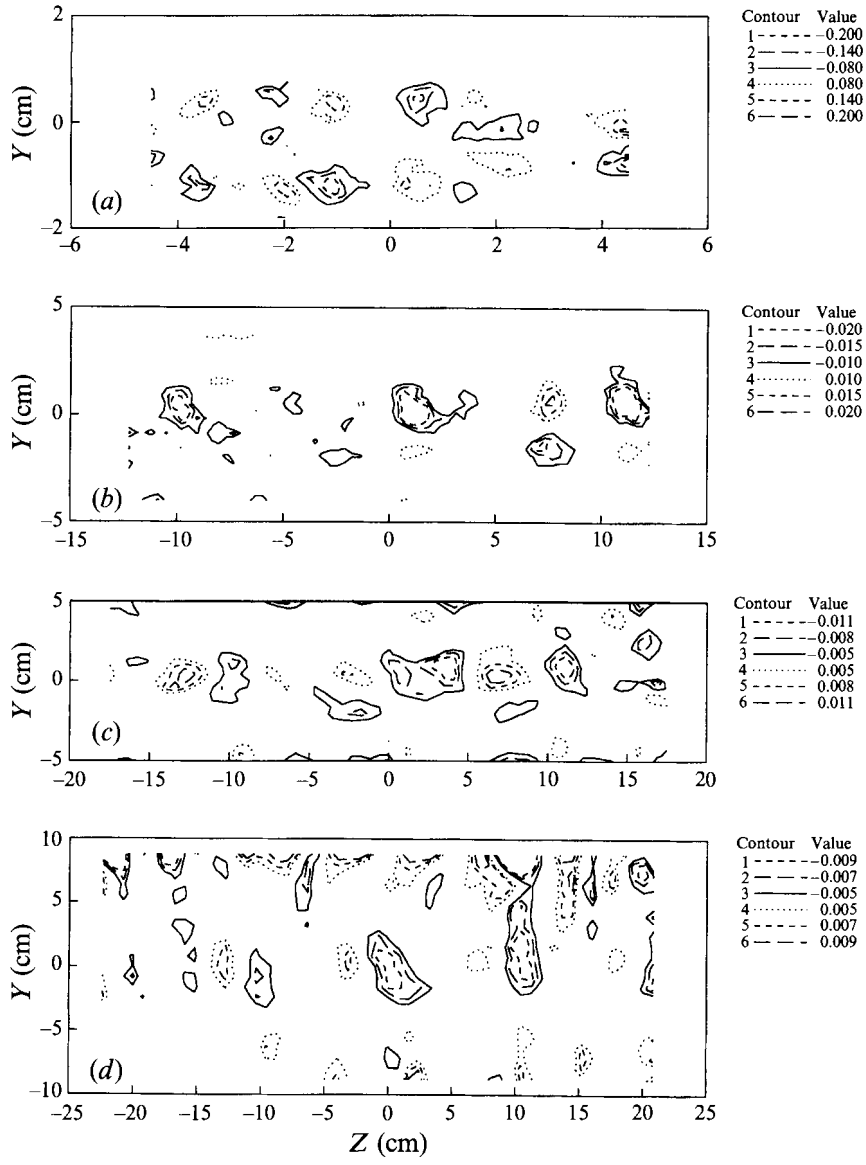

FIGURE 13. Mean streamwise vorticity (Ω_x/U_e, cm^{-1}) contours for the curved untripped wake: (*a*) $X = 11$ cm; (*b*) $X = 76$ cm; (*c*) $X = 125$ cm; (*d*) $X = 254$ cm.

disturbances. It was found that the locations of the quadrupoles were weakly correlated with extrema in the spanwise distribution of the boundary layer skin friction coefficient on the splitter plate (Weygandt & Mehta 1993). A similar correlation was observed earlier in some straight mixing layer studies (Bell & Mehta 1992). In agreement with the straight wake results, the quadrupole positions in the curved wake coincide approximately with the crest/pinch locations in the mean velocity contours.

At the first station, the peak levels of mean streamwise vorticity on the stable and unstable sides of the wake are comparable. However, by $X = 76$ cm (figure 13*b*), the quadrupoles are becoming harder to discern since they are in the process of transforming into a single row of counter-rotating vortices; the vortices on the unstable (higher-Y) side persist while those on the stable side have decayed. This trend continues

with downstream distance and at $X = 125$ cm and 254 cm (figures 13*c* and 13*d*) only a single row of counter-rotating mean vorticity remains on the unstable side of the wake. Note that the apparent structures at the edge of the measurement domain are remnants of noise introduced by the vorticity evaluation scheme. As in the straight wake, the peak mean streamwise vorticity on both sides of the curved wake decays with increasing streamwise distance and the spacing between the vortical structures also increases.

As stated above in §3.1, the distortions in the far-field mean velocity and Reynolds stress contours were trackable from one station to the next in the straight untripped wake, but not in the curved one. The reason for this difference is related to the difference in the decay of mean streamwise vorticity seen in the two cases. The initial pattern of spanwise variation in the contours is determined by the near-field distribution of mean streamwise vorticity. As the location and scale of the streamwise vorticity change with streamwise distance, so does the distortion pattern. In the straight case, once the mean streamwise vorticity has decayed completely on both sides of the wake (by $X = 128$ cm), the spanwise distortion is 'locked-in' and there is no mechanism to change it further downstream. In the curved case, however, the mean streamwise vorticity decays on the stable side, but persists on the unstable side, and thus changes related to this single row of streamwise vorticity continually change the pattern of the spanwise variation. The persistence of streamwise vorticity on the unstable side is also responsible for the stronger variations on that side of the curved wake.

Mean streamwise vorticity contours are not presented here for either of the tripped cases since no spatially stationary streamwise vortical structures, such as those in the untripped cases, were measured. This is consistent with the nominally two-dimensional behaviour of the velocity contours and wake properties for both tripped cases (figures 5*b*, *d* and 6*b*, *d*). The lack of mean streamwise vorticity in the curved tripped case is particularly noteworthy since it demonstrates that mild curvature alone does not generate a (mean) three-dimensional structure in the wake. The time-averaged measurement techniques used in this study may mask the presence of temporally variant streamwise vortices. Only spatially stationary streamwise vortices with long lifetimes are resolved using the present measurement techniques. Thus, for a structure to be identified, it must be spatially stationary and make a continuous contribution to the secondary velocities over the, relatively long, full data acquisition time. So it is possible that streamwise vorticity is generated in the tripped cases, but not detected in the present time-averaged measurements. However, in a recent direct numerical simulation of a time-developing turbulent (tripped) wake, streamwise or 'rib' vortices were not identified at all (Rogers & Moser 1993*b*; Moser & Rogers 1994). This was attributed to the absence of organized spanwise structures with well-defined braid regions, where the rib vortices develop.

Although the generation of streamwise vortical structures in the untripped cases is not significantly affected by curvature, their streamwise evolution certainly is influenced. The streamwise evolution of some of the global properties of the mean streamwise vorticity is presented in figures 14–16.

Th streamwise development of the peak mean streamwise vorticity is plotted on a log–log scale in figure 14. The magnitude of the peak mean vorticity at each station is obtained by averaging the maximum absolute values of all of the identified vortices. Since the two rows of vortices in the straight wake decayed at approximately the same rate, only their average is plotted in figure 14, but the results for the two sides of the curved case (stable and unstable) are presented individually. Initially, the peak vorticity

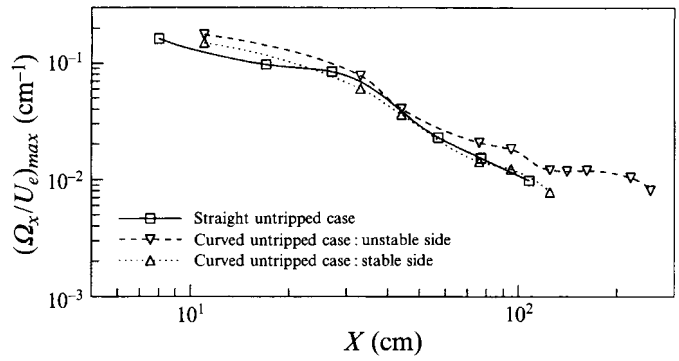

FIGURE 14. Streamwise development of peak mean streamwise vorticity.

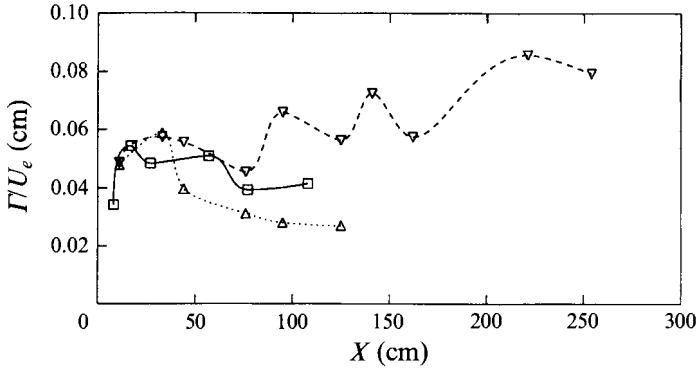

FIGURE 15. Streamwise development of average streamwise vortex circulation. Curves defined as in figure 14.

levels are comparable for the three cases, especially if the curved results are extrapolated back to $X = 8$ cm. In the near-field region ($X = 10$–30 cm), based on the fit to the data, the peak levels in the curved wake are higher than those in the straight wake. This is why the distortions in the mean velocity and Reynolds stress contours (figures 3–8) are more severe in the curved wake. By $X = 40$ cm, the peak levels for all three cases are comparable, but further downstream the rate of decay for the unstable side of the curved wake is clearly much lower than those of the straight and stable cases. Between $X = 30$ and 100 cm, the peak mean vorticity in the straight and stable cases decays as approximately $X^{-1.2}$. The slower decay of the unstable side results in the transformation of the quadrupoles into a single row of counter-rotating vortices residing only on the unstable side, as shown in the mean streamwise vorticity contours in figure 13. This effect of curvature in retarding the decay of mean streamwise vorticity on the unstable side of the wake was also observed in some earlier studies of a curved (unstable) mixing layer (Plesniak *et al.* 1994).

The streamwise development of the average circulation per vortical structure for the untripped cases is presented in figure 15. The circulation for each structure is evaluated as described in §2, and the absolute values are then averaged over all the structures at a given streamwise location. The average circulation for the straight case decreases slowly with a temporary small rise at $X \approx 50$ cm. The stable side circulation falls-off more rapidly in this region after the initial rise. The unstable side circulation shows a similar behaviour in the near-field region, but then beyond $X \approx 75$ cm, there is generally an increasing trend, with temporary drop-offs. Temporary jumps in the

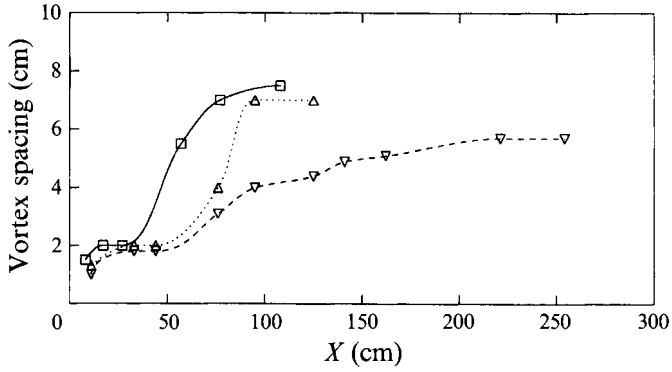

FIGURE 16. Streamwise development of mean streamwise vortex spacing. Curves defined as in figure 14.

average circulation per vortex have been previously observed in both straight (Bell & Mehta 1992) and curved (Plesniak *et al.* 1994) mixing layer studies where they were attributed to viscous amalgamation or annihilation of pairs of streamwise vortices. Similar interactions could also be responsible for the trends observed here, as further discussed below. In terms of the effects of curvature, destabilizing curvature increases the average circulation (beyond $X \approx 75$ cm), while stabilizing curvature decreases it, compared to that in the straight case. Exactly the same trends were observed in the curved mixing layer studies (Plesniak *et al.* 1994), although the mechanisms responsible for the effects are not apparent.

The development of the mean spacing of the streamwise vortices, obtained by dividing the measured span by the number of identified vortices in each row, is presented in figure 16. The straight wake spacing represents an average for the two sides of the straight wake. In general, all three curves show an increasing trend in the spacing, but in a stepwise fashion. The increasing spacing was, of course, expected since the wavelengths of the distortions in the mean velocity and Reynolds stress contours increased with streamwise distance. In the very near field ($X < 30$ cm), the spacing for all three cases is very similar. However, further downstream, the spacing for the straight case increases first, followed by that for the stable side and then the unstable. It is interesting to note that the stepwise increase in spacing and the fact that the unstable side has the lowest spacing is very similar to what was observed in the curved mixing layer studies (Plesniak *et al.* 1994). The fact that the sudden rises in spacing are, in general, approximately coincident with the sharp changes in average circulation gives credence to the streamwise vortex amalgamation/annihilation theory. Note that pairing of the spanwise vortices, which will not typically occur in an unforced wake, is not essential for the streamwise vortex interaction, and hence scale change, to occur (Rogers & Moser 1993*a*).

3.3. *Streamwise evolution of the wake defect and half-width*

The streamwise development of the spanwise-averaged wake defect for the straight and curved wakes with both initial conditions is compared in figure 17. In the far-field region (beyond $X = 50$ cm), the defect is clearly only a function of the initial conditions, with that for the tripped cases being substantially greater. In the near-field region ($X < 30$ cm), the defect for the straight untripped wake is equivalent to that of the tripped cases. However, further downstream it decays at a faster rate than that in the tripped cases and becomes equivalent to the defect in the curved untripped wake.

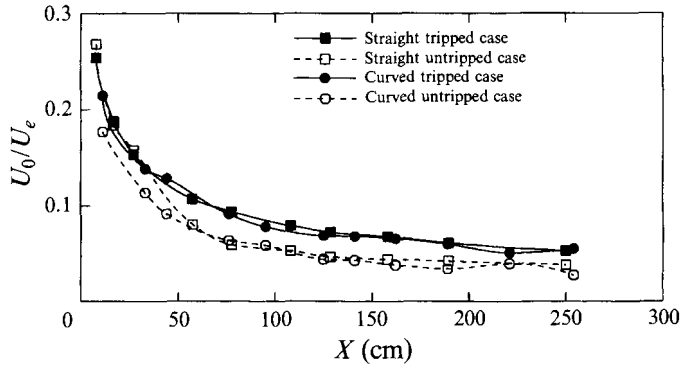

FIGURE 17. Streamwise development of wake defect.

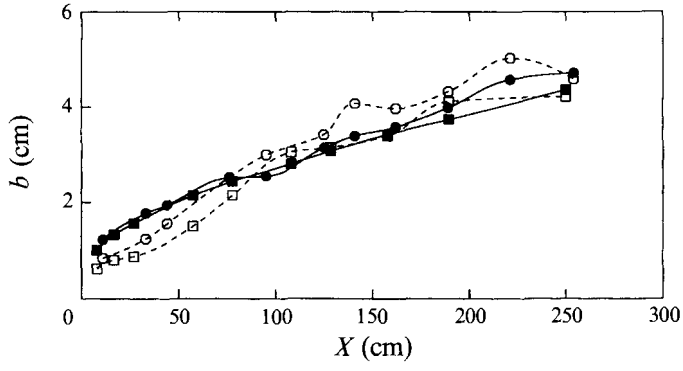

FIGURE 18. Streamwise development of wake half-width. Curves defined as in figure 17.

For the same initial conditions, the curved untripped wake defect is lower at $X = 11$ cm than in the straight untripped case, implying that curvature must have produced a faster defect decay rate upstream of $X = 11$ cm. The faster defect decay observed in both the untripped wakes is attributed to the presence and action of the organized (spatially stationary) streamwise vortices which produce additional entrainment that fills-in the defect faster. This additional entrainment is absent in the tripped wakes since streamwise vorticity is not generated in these cases. That the decay in the velocity defect is faster in the near wake of the untripped curved wake (compared to that in the untripped straight wake) implies that the effects of streamwise vorticity are stronger in the very near-field region of the curved case. In fact, as shown in figure 14, the peak mean streamwise vorticity is higher in the curved wake at $X = 11$ cm. The faster rate of defect decay in the untripped cases persists only to about $X = 77$ cm. Further downstream, the rate of decay for the untripped cases is comparable to that of the tripped cases, because of the mean streamwise vorticity, and its associated affects, weakening with streamwise distance. The streamwise development of the defect for the straight tripped wake agreed well with the half-power-law relation for a self-similar wake obtained by assuming a constant eddy viscosity (Ramaprian, Patel & Sastry 1982; Weygandt & Mehta 1993).

Although not discussed specifically, the results of Ramjee *et al.* (1988) and Ramjee & Neelakandan (1989, 1990) for airfoil wakes showed a lower defect in the untripped airfoil wake compared to that for the tripped case, in agreement with the present findings. However, in contrast to the present findings, they found that the wakes of a symmetric airfoil and a rectangular cylinder had higher defects in the curved cases than

in the straight ones. They also showed that the relative increase in defect due to the imposition of streamwise curvature was related to the ratio of curvature ($b/\bar{R}$), with the defect increasing with ratio of curvature. It is not obvious, intuitively, why the defect should increase with curvature and Ramjee *et al.* did not offer any explanations either. On the other hand, Koyama (1983) reported that the defect of his curved wake was lower than that of the straight wake. Again, the possible reasons for this effect were not discussed.

The streamwise development of the spanwise-averaged wake half-width for the four cases is presented in figure 18. The straight and curved tripped half-widths exhibit similar levels and development in the near-field region. However, beyond about $X = 100$ cm, the curved tripped half-width grows faster than that of the straight tripped wake and the overall half-width for the curved case is about 10% higher at the last measurement location ($X \approx 250$ cm). Just downstream of the trailing edge of the splitter plate, both the straight and curved untripped wakes are thinner than the tripped wakes. However, the untripped cases grow at a faster rate in the near-field region and their thicknesses are soon comparable to, or higher than, those of the tripped wakes. The higher growth rate of the untripped cases is again attributed to additional entrainment by the spatially stationary streamwise vortices. In the far-field region, the growth rates of the two untripped cases appear similar, but the overall half-width of the curved untripped wake is about 20% higher. The straight untripped case half-width is about the same as that of the straight tripped case in the far wake, implying that in the absence of streamwise curvature, the far-wake half-width is not as strongly influenced by the history of initial conditions as the velocity defect is. However, the curved untripped half-width is about 10% greater than the curved tripped half-width in the far wake, suggesting that the combination of streamwise curvature and streamwise vorticity produce a higher wake growth rate in the near wake, and hence, a higher overall half-width in the far-field region. So clearly, the effects of curvature on the untripped wake manifest themselves in a complex manner and cannot be simply thought of as a superposition of the effects of streamwise curvature and those of streamwise vorticity. As with the velocity defect, the half-width of the straight tripped case also exhibited self-similar behaviour (Weygandt & Mehta 1993).

Another point to note is that there is some scatter in the untripped wake distributions, especially in the far-field regions. One possible factor responsible for this behaviour is related to the issue of spanwise convergence. At each streamwise location, the spanwise extent of the measurement domain was chosen so that it covered approximately ten local half-widths. Now as discussed above in §3.1, the wavelength of the spanwise variation in half-width for both untripped cases increases with streamwise distance. Therefore, it is possible that, in the far-field region, not enough wavelengths of the variation were covered to assure convergence of the spanwise-averaged half-width.

The contribution to the total half-width of the individual wake sides or halves for the tripped cases are shown in figure 19. In the curved untripped case, no obvious trend was apparent owing to the scatter resulting from the spanwise convergence problem discussed above and also owing to uncertainty in determining the centreline position. The straight wake half-half-width (b') was determined by merely halving the overall half-width given in figure 18. However, the unstable and stable side contributions in the curved cases are not the same owing to the effects of curvature and the half-half-width of each side was, therefore, determined individually. The distributions clearly show that, beyond $X \approx 100$ cm, the curved wake half-half-width on the unstable side is

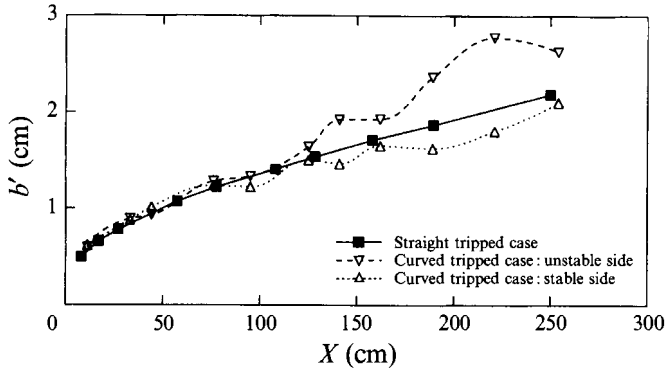

FIGURE 19. Streamwise development of wake half-half-width.

increased relative to that of the straight case, while that on the stable side is decreased. Of course, the effects are much stronger on the unstable side which is why the overall curved wake half-width is increased (figure 18). The present results regarding the effects of curvature on the half-half-width are in qualitative agreement with those of Ramjee *et al.* (1988) and Ramjee & Neelakandan (1989, 1990).

3.4. *Reynolds stress profiles in similarity coordinates*

In order to further examine the effects of initial conditions and curvature on the turbulent structure of the wake, spanwise-averaged Reynolds stress profiles, plotted in similarity coordinates, are presented for all four cases in figures 20–23. The Reynolds stresses are normalized by the velocity defect, U_0, and η is defined as $(Y-Y_0)/b$, where Y_0 is the location of the wake centreline. For the spanwise averaging, each Y-profile was reduced individually using its own velocity defect and half-width, before being spanwise averaged onto a uniform grid. Note that since the stress levels in the untripped cases, especially in the near-field regions, are typically much higher than those in the tripped cases, the vertical scales for the two initial conditions are not the same.

Since there are the two regions of maximum mean shear $(\partial U/\partial Y)$ in a wake, on either side of the centreline, the Reynolds stress distributions should be expected to exhibit two peaks. The $\overline{u'^2}$ profiles exhibit the characteristic double-peaked profile shape for the tripped cases, but not for the untripped ones, at least not downstream of the first one or two stations (figure 20). A part of the reason for this absence is that, with the large spanwise variations in the untripped cases, the double-peaks tend to get washed-out when the spanwise averaging is applied. Another notable difference between the tripped and untripped wakes is that regarding the streamwise development of $\overline{u'^2}$. The peak level of $\overline{u'^2}$ is relatively low in the very near field of all four cases, and while the peak levels in the untripped cases achieve a local maximum in the near-field region, those for the tripped cases increase monotonically. The $\overline{u'^2}$ profiles in the straight cases achieve some degree of collapse in the far-field region, with the maximum levels comparable, but those for the curved cases are clearly still evolving. The profiles for the straight cases are nominally symmetric about the centreline ($\eta = 0$), but those for the curved cases become asymmetric such that in the far field, the peak level on the unstable side ($\eta > 0$) of the curved tripped wake is higher than that of the straight tripped wake, while that on the stable side is lower. In the untripped curved wake, the single-peaked profile becomes asymmetric such that the peak shifts towards the unstable side and the maximum levels are considerably higher than those in the straight

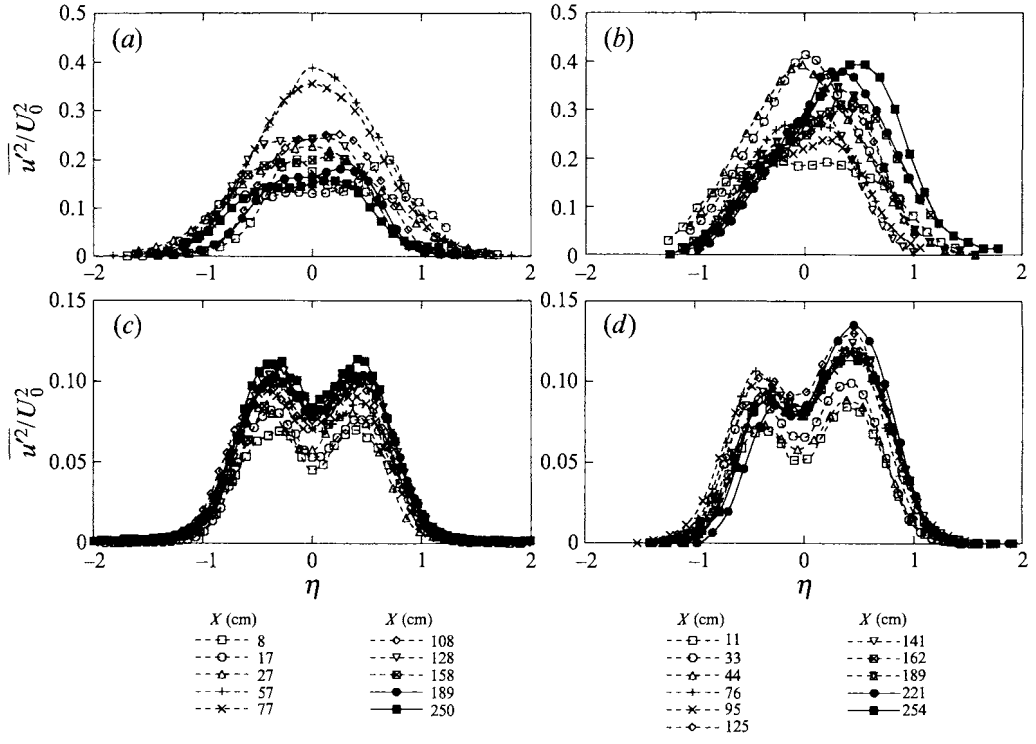

FIGURE 20. Streamwise normal stress profiles in similarity coordinates: (*a*) straight untripped wake; (*b*) curved untripped wake; (*c*) straight tripped wake; (*d*) curved tripped wake.

untripped wake. The present results on the effects of curvature on $\overline{u'^2}$ are in agreement with those of Ramjee & Neelakandan (1990), but not with some of the other previous measurements. Savill (1983) and Koyama (1983) reported that their $\overline{u'^2}$ profiles in the curved wake remained symmetric and the peak levels were lower in the curved wake, whereas Nakayama (1987) found that $\overline{u'^2}$ increased on the stable side of his curved wake.

The $\overline{v'^2}$ profiles (figure 21) for all cases exhibit a double-peaked profile in the very near-field region (especially in the untripped cases), but this is quickly washed away and the profiles further downstream have a single peak. Pot (1979) and Jovic & Ramaprian (1986) also reported a double-peak in the very near wake which washed-out further downstream. The washing-out of the double peaks is related to the passage of the spanwise vortices. The passage of each vortex produces a strong v-fluctuation which would fill-in the dip of the double-peaked profile along the centreline of the wake. As with the $\overline{u'^2}$ distributions, the peak $\overline{v'^2}$ levels for the straight untripped case decrease monotonically with increasing streamwise distance while those for the straight tripped case increase and achieve an approximately constant level in the far-field region. The maximum levels of $\overline{v'^2}$ at the last station ($X = 250$ cm) are comparable for the two straight cases. The peak $\overline{v'^2}$ levels in the curved untripped case also decrease initially, but then increase monotonically beyond $X = 95$ cm, as do those in the curved tripped wake. Furthermore, the $\overline{v'^2}$ profiles in both the curved cases clearly become asymmetric with the peak biased towards the unstable side ($\eta > 0$). Savill (1983), Nakayama (1987) and Ramjee & Neelakandan (1989) found similar effects of curvature on $\overline{v'^2}$ in their curved wake studies.

The behaviour of the $\overline{w'^2}$ profiles (figure 22) is very similar to that of the $\overline{u'^2}$ profiles.

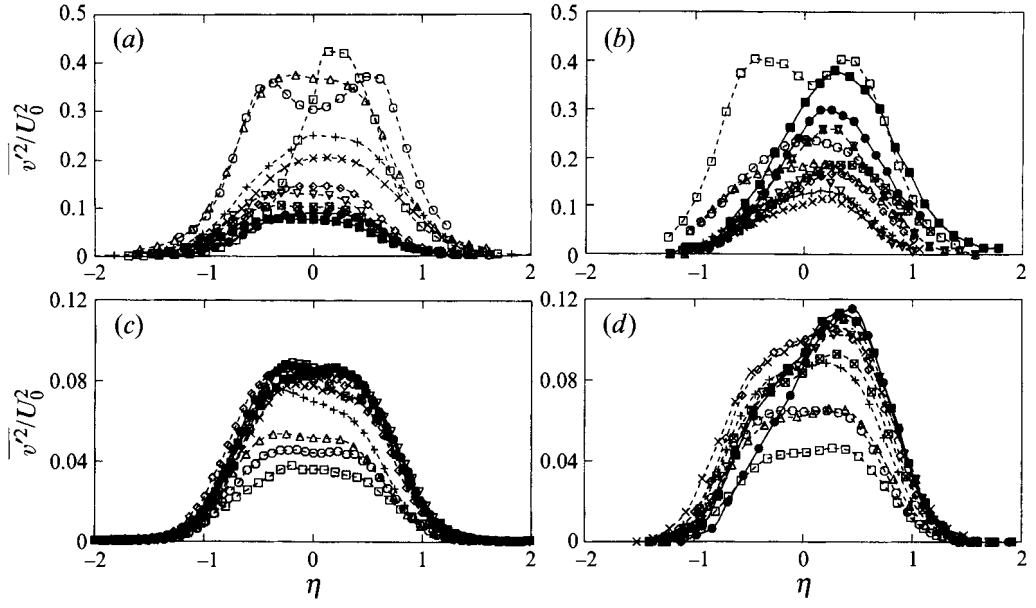

FIGURE 21. Cross-stream normal stress profiles in similarity coordinates: (*a*) straight untripped wake; (*b*) curved untripped wake; (*c*) straight tripped wake; (*d*) curved tripped wake. Curves defined as in figure 20.

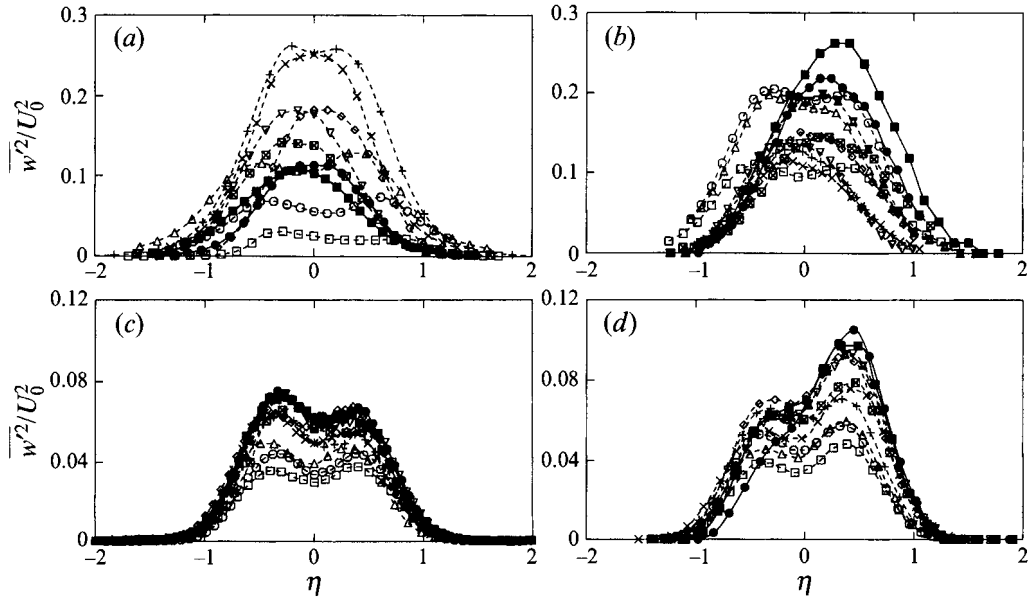

FIGURE 22. Spanwise normal stress profiles in similarity coordinates: (*a*) straight untripped wake; (*b*) curved untripped wake; (*c*) straight tripped wake; (*d*) curved tripped wake. Curves defined as in figure 20.

Once again, downstream of $X \approx 40$ cm, the double-peaked profiles are only apparent in the tripped cases. For both untripped cases, the peak $\overline{w'^2}$ increases with streamwise distance, achieves a maximum in the intermediate-wake region and then decreases again. In the straight untripped wake, the peak $\overline{w'^2}$ continues to decrease monotonically, but that in the curved tripped wake increases in the far-field region

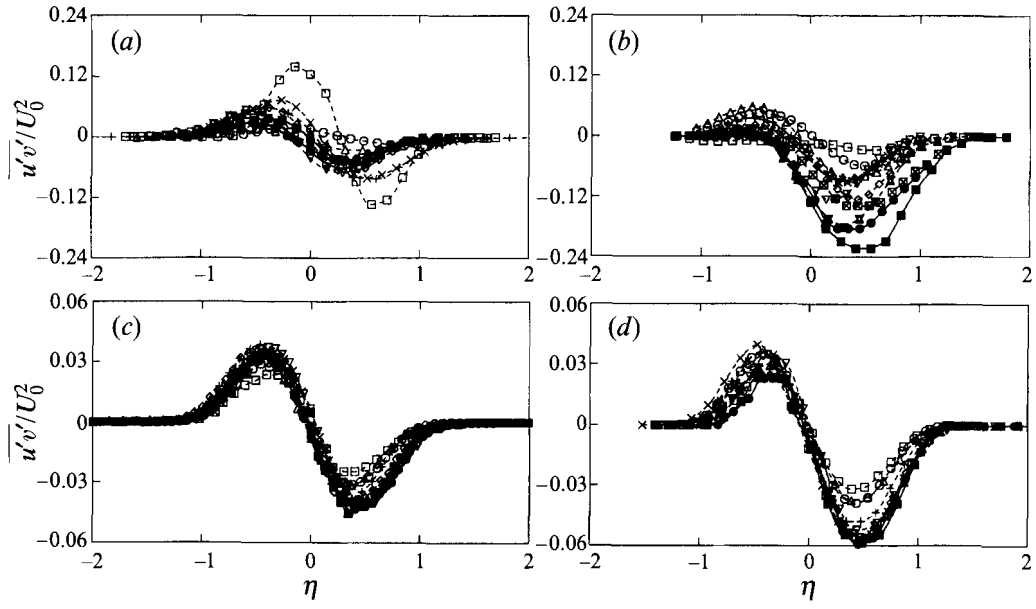

FIGURE 23. Primary shear stress profiles in similarity coordinates: (*a*) straight untripped wake; (*b*) curved untripped wake; (*c*) straight tripped wake; (*d*) curved tripped wake. Curves defined as in figure 20.

owing to the effects of curvature. The peak $\overline{w'^2}$ levels in both tripped cases increase with streamwise distance, and the profiles for the straight tripped wake collapse well in the far-field region. The asymmetry in the profiles for the curved cases is again clearly apparent, as are the increased $\overline{w'^2}$ levels on the unstable side of the wake and reduced levels on the stable side. At least the reduction of $\overline{w'^2}$ on the stable side was also observed by Savill (1983).

The effects of curvature are most apparent in the primary shear stress ($\overline{u'v'}$) profile measurements (figure 23). The familiar antisymmetric distributions with approximately equal peak magnitudes on the two sides of the wake are exhibited for the straight cases. The profiles for the straight tripped wake show good collapse in the far-field region, thus exhibiting a tendency toward a self-similar state. The profiles for the curved cases clearly show the effects of curvature; the levels on the stable side are reduced compared to those in the corresponding straight wake, while those on the unstable side are increased significantly. This observation is in general agreement with that from all previous studies on curved wakes (Savill 1983; Nakayama 1987; Ramjee & Neelakandan 1989, 1990). It is noteworthy that the asymmetry in levels on the two sides of the curved wake is developed almost as soon as the mild curvature is applied. Also note that the peak ($\overline{u'v'}$) levels continue to increase with streamwise distance on the unstable side while those on the stable side continue to decrease. In fact, in the curved untripped wake, the positive shear stress on the stable side has been almost completely obliterated!

The Reynolds stress profiles presented above bring out three main points. First, the effects of curvature on the Reynolds stress distributions are quite severe and they are apparent right from the first station ($X = 11$ cm), especially in the tripped case. This is particularly significant in view of the mildness of the imposed curvature ($b/\bar{R} < 2\%$). Also, all four Reynolds stress components show similar effects due to curvature, whereby the profiles become asymmetric and the peak levels on the unstable side of the

wake are increased significantly, whereas those on the stable side are reduced, compared to those in the straight wake. Also, the effects of curvature on the Reynolds stresses continue to manifest themselves up to the last measurement location. This is because the ratio of curvature ($b/\bar{R}$) increases as the wake grows, and thus the effects of curvature are expected to become more pronounced with increasing downstream distance. In the untripped case, the ratio of curvature ranges from 0.3% at $X = 11$ cm to 1.6% at $X = 254$ cm, while in the tripped case it ranges from 0.4% to 1.6% at the same two locations.

The second point borne out by the present results is that the effects of curvature are much stronger on the untripped wake. For example, the stress levels on the unstable side of the untripped wake are significantly higher than those on the unstable side of the tripped wake. A part of this disparity is obviously due to the difference in the normalizing velocity (wake defect) which, for a given streamwise location, is lower in the untripped cases. However, on examining the raw (unnormalized) stress data, it was found that even the raw stresses were higher on the unstable side of the untripped wake compared to those in the tripped wake. The additional production of Reynolds stress can be attributed to the presence of mean three-dimensionality in the untripped cases, as discussed below in §3.5.

Thirdly, of the two straight wake cases, only the tripped wake exhibits an asymptotic behaviour in the far-field region with the Reynolds stress profiles collapsing adequately. This, together with the wake defect and half-width following the half-power-laws (§3.3), shows that the straight tripped wake has achieved a self-similar state. Although the peak Reynolds stress levels at the last station in the straight untripped wake are approaching those of the tripped case, it is clear that this wake is still recovering from transition and mean three-dimensionality. The curved tripped wake cannot be expected to behave in a self-similar manner because of the following argument. Strictly speaking, the curvature effects on turbulence are described by the rate-of-strain ratio, $1/S = (\partial V/\partial X)/(\partial U/\partial Y)$ (Bradshaw 1973). The $\partial V/\partial X$ term is proportional to $U/\bar{R}$, and the $\partial U/\partial Y$ term is proportional to U_0/b. Thus, the rate-of-strain ratio, approximated as $[(b/\bar{R})(U/U_0)]$, is constantly increasing. As the wake develops, the half-width grows and the defect decays, and thus the only way the ratio could be maintained constant would be for the radius of curvature to increase in a corresponding manner, which would obviously require a spiralling test section!

3.5. *Reynolds stress transport equations*

The changes in stress levels observed on the stable and unstable sides of the curved wake can be attributed, at least in part, to extra production terms in the Reynolds stress transport equations which are activated by the angular momentum instability. The effects of streamwise curvature can also arise implicitly through changes in the turbulence structure which can act to enhance or suppress turbulence production – these are often referred to as 'higher-order' effects. The abbreviated forms of the transport equations for five of the Reynolds stresses ($\overline{u'^2}$, $\overline{v'^2}$, $\overline{w'^2}$, $\overline{u'v'}$ and $\overline{u'w'}$) are presented below (equations (3.1) to (3.5)). The terms for pressure diffusion (*PD*), pressure–strain correlation (*PS*), viscous diffusion (*VD*), and viscous dissipation (*D*) are represented only symbolically. The transport equations presented below are based on the 'fairly thin shear layer' approximation of Bradshaw (1973) (i.e. $b/\bar{R}$ is assumed small but not negligible). Since the untripped wakes exhibit a three-dimensional mean structure, terms involving spanwise gradients ($\partial/\partial Z$) and the secondary Reynolds shear stresses ($\overline{u'w'}$ and $\overline{v'w'}$) are retained. Terms involving gradients in the normal and spanwise directions of the secondary mean velocities (V and W) are also retained for

the same reason. The terms on the right-hand side of the first line represent production or generation, those on the second line represent production arising from three-dimensionality of the mean flow, and those on the third line represent turbulence transport by turbulent diffusion. The underlined terms in (3.1), (3.2) and (3.4) are not true production terms, but arise from rotation of the coordinate axes (Bradshaw 1973).

$$\frac{\mathrm{D}}{\mathrm{D}t}\left(\frac{\overline{u'^2}}{2}\right) = -\overline{u'^2}\left(\frac{\partial U}{\partial X}+\frac{V}{R}\right)-\overline{u'v'}\left[\left(1+\frac{Y}{R}\right)\frac{\partial U}{\partial Y}-\frac{U}{R}\right]-\underline{2\overline{u'v'}\frac{U}{R}}$$
$$-\overline{u'w'}\frac{\partial U}{\partial Z}$$
$$-\frac{\partial}{\partial X}\left(\frac{\overline{u'^3}}{2}\right)-\frac{\partial}{\partial Y}\left[\left(1+\frac{Y}{R}\right)\left(\frac{\overline{u'^2v'}}{2}\right)\right]-\frac{\overline{u'^2v'}}{R}-\frac{\partial}{\partial Z}\left(\frac{\partial u'^2w'}{2}\right)$$
$$+PD+PS+VD+D, \tag{3.1}$$

$$\frac{\mathrm{D}}{\mathrm{D}t}\left(\frac{\overline{v'^2}}{2}\right) = -\overline{v'^2}\left(1+\frac{Y}{R}\right)\frac{\partial V}{\partial Y}-\overline{u'v'}\frac{\partial V}{\partial X}+\underline{2\overline{u'v'}\frac{U}{R}}$$
$$-\overline{v'w'}\frac{\partial V}{\partial Z}$$
$$-\frac{\partial}{\partial X}\left(\frac{\overline{u'v'^2}}{2}\right)-\frac{\partial}{\partial Y}\left[\left(1+\frac{Y}{R}\right)\left(\frac{\overline{v'^3}}{2}\right)\right]-\frac{\overline{u'^2v'}}{R}-\frac{\partial}{\partial Z}\left(\frac{\overline{v'^2w'}}{2}\right)$$
$$+PD+PS+VD+D, \tag{3.2}$$

$$\frac{\mathrm{D}}{\mathrm{D}t}\left(\frac{\overline{w'^2}}{2}\right)+0$$
$$-\overline{u'w'}\frac{\partial W}{\partial X}-\overline{v'w'}\left(1+\frac{Y}{R}\right)\frac{\partial W}{\partial Y}-\overline{w'^2}\frac{\partial W}{\partial Z}$$
$$-\frac{\partial}{\partial X}\left(\frac{\overline{u'w'^2}}{2}\right)-\frac{\partial}{\partial Y}\left[\left(1+\frac{Y}{R}\right)\left(\frac{\overline{v'w'^2}}{2}\right)\right]-\frac{\partial}{\partial Z}\left(\frac{\overline{w'^3}}{2}\right)$$
$$+PD+PS+VD+D, \tag{3.3}$$

$$\frac{\mathrm{D}}{\mathrm{D}t}(\overline{u'v'}) = -\overline{u'^2}\left(\frac{\partial V}{\partial X}-\frac{U}{R}\right)-\overline{v'^2}\left(1+\frac{Y}{R}\right)\frac{\partial U}{\partial Y}-\underline{(\overline{u'^2}-\overline{v'^2})\frac{U}{R}}$$
$$-\overline{u'w'}\frac{\partial V}{\partial Z}-\overline{u'v'}\frac{\partial W}{\partial Z}-\overline{v'w'}\frac{\partial U}{\partial Z}$$
$$-\frac{\partial}{\partial X}(\overline{u'^2v'})-\left(1+\frac{Y}{R}\right)\frac{\partial}{\partial Y}(\overline{u'v'^2})-2\frac{\overline{u'v'^2}-\overline{u'^3}}{R}-\frac{\partial}{\partial Z}(\overline{u'v'w'})$$
$$+PD+PS+VD+D, \tag{3.4}$$

$$\frac{\mathrm{D}}{\mathrm{D}t}(\overline{u'w'}) = -\overline{v'w'}\left(1+\frac{Y}{R}\right)\frac{\partial U}{\partial Y}-\overline{v'w'}\left(\frac{U}{R}\right)+\overline{u'w'}\left(1+\frac{Y}{R}\right)\frac{\partial V}{\partial Y}$$
$$-\overline{u'v'}\left(1+\frac{Y}{R}\right)\frac{\partial W}{\partial Y}-\overline{u'^2}\frac{\partial W}{\partial X}-\overline{w'^2}\frac{\partial U}{\partial Z}$$
$$-\frac{\partial}{\partial X}(\overline{u'^2w'})-\left(1+\frac{Y}{R}\right)\frac{\partial}{\partial Y}(\overline{u'v'w'})-\frac{\partial}{\partial Z}(\overline{u'w'^2})$$
$$+PD+PS+VD+D. \tag{3.5}$$

With the defined coordinate system, $\partial U/\partial Y > 0$ and $\overline{u'v'} < 0$ on the unstable side of the curved wake, while $\partial U/\partial Y < 0$ and $\overline{u'v'} > 0$ on the stable side. Since the rate of strain ratio, S, approximated as $(U/\bar{R})/(\partial U/\partial Y)$, is defined negative for the unstable side and positive for the stable side, $U/\bar{R} < 0$ for both sides. In terms of the effects of curvature, for the normal stress $\overline{u'^2}$ the additional production terms due to streamwise curvature are:

$$-\overline{u'v'}\left[\left(1+\frac{Y}{R}\right)\frac{\partial U}{\partial Y}-\frac{U}{R}\right].$$

The factor $(1 + Y/R)$ is always positive, regardless of the sign of Y, and approximately equal to 1 since $R \gg Y$. So the production due to the first term in the square brackets is not much affected by curvature and it contributes positively to $\overline{u'^2}$ on both sides of the wake. However, the second term in the square brackets contributes positively on the unstable side and negatively on the stable side, thus producing the asymmetric distribution of $\overline{u'^2}$ seen in figures 20(*b*) and 20(*d*).

The similarity coordinate profiles for $\overline{v'^2}$ and $\overline{w'^2}$ for the curved wakes also show some asymmetry, both in shape and peak levels, between the two sides of the wake (figures 21*b*, *d* and 22*b*, *d*). However, there are no significant additional production terms due to curvature in (3.2) and (3.3), although for $\overline{v'^2}$, the term, $\overline{u'v'}(\partial V/\partial X)$ could play a role since $\partial V/\partial X$ can be approximated as $-U/\bar{R}$ (Bradshaw 1973). This production term will then contribute positively to $\overline{v'^2}$ on the unstable side and negatively on the stable side. All of the changes in $\overline{w'^2}$, and at least some in $\overline{v'^2}$, due to curvature must, therefore, be attributed to higher-order effects. It is these types of effects, which are not accounted for in the transport equations, that make the computation of such turbulent flows even more difficult.

For the primary shear stress, $\overline{u'v'}$, the additional production terms arising due to curvature are:

$$-\overline{u'^2}\left(\frac{\partial V}{\partial X}-\frac{U}{R}\right)-\overline{v'^2}\left(1+\frac{Y}{R}\right)\frac{\partial U}{\partial Y},$$

where $\partial V/\partial X$ can again be approximated by $-U/\bar{R}$. As discussed above, the second term accounts for the 'normal' production of $\overline{u'v'}$, positive on the stable side and negative on the unstable side. The first term contributes negative levels on both sides of the curved wake, thus increasing the magnitude of the negative shear stress on the unstable side while decreasing the positive level on the stable side.

As discussed above in §3.4, the effects of curvature are more severe on the curved untripped wake than on the curved tripped case. Not only are the normalized Reynolds stress levels (figures 20*b*, *d*–23*b*, *d*) considerably higher in the untripped case, but the raw (unnormalized) stresses were found to be as well (Weygandt & Mehta 1993). This difference can be attributed to the mean three-dimensionality of the untripped wake. The presence and persistence of streamwise vorticity produces significant spanwise variations in the mean velocity contours (figure 3), secondary velocities (V and W) and gradients thereof. Moreover, significant levels of the secondary shear stress, $\overline{u'w'}$, are also generated in the curved untripped wake (figure 11). This means that the second lines in (3.1)–(3.5), representing Reynolds stress production due to mean three-dimensionality, would also contribute significantly in the curved untripped wake, thus leading to higher stress levels.

4. Conclusions

A study of the three-dimensional structure of straight and curved plane wakes at relatively high Reynolds numbers ($Re_b = 28000$) with tripped and untripped initial boundary layers has been completed. The straight and curved wakes with untripped initial boundary layers are grossly three-dimensional in the near-field region with large spanwise variations in the mean velocity and Reynolds stress contours. The spanwise variation is observed in the form of pinches and crests in the contour lines which result in a significant variation in the spanwise distribution of the wake half-width and defect. This type of distortion is generated by the presence of quadrupoles of spatially stationary streamwise vorticity. In the Reynolds stress contours, the spanwise variation also exhibits local peaks which appear in a quasi-periodic manner and coincide approximately with regions of maximum velocity defect. The spanwise variation in the Reynolds stress distributions cannot be removed by normalizing by the local defect, thus suggesting a high degree of complexity in the form of the three-dimensionality.

In contrast to the mixing layer, where this type of three-dimensionality is also generated (Bell & Mehta 1992), the wake is slow to recover from the initial perturbations. The mixing layer is constantly energized by the velocity difference, and thus relatively strong turbulent mixing tends to wash-out a disturbance quickly. However, the wake is of a diffusive or dying nature, and hence relatively slow to recover. The spanwise variations are found to persist into the far-field regions of the wake, although they certainly decrease in magnitude with increasing streamwise distance. This is despite the fact that the mean streamwise vorticity has decayed completely by the far wake in the straight case and partially in the curved case. In the straight case, the contours exhibit a readily apparent consistency or trackability of spanwise variation in the far-field region, as the pattern becomes locked-in once the mean streamwise vorticity has decayed completely. However, the distortions in the curved case contours are not as trackable, since significant mean streamwise vorticity, and related scale changes, persist on the unstable side.

The mechanisms responsible for the formation of streamwise vorticity in plane wakes are expected to be similar to those in mixing layers, since the same structural features (spanwise vortices and braids) are present in both shear flows. However, since the Kármán vortex street is composed of two rows of alternating-signed spanwise vortices, both untripped wakes correspondingly developed two rows of alternating-signed vortices arranged in quadrupoles. The initial locations of the quadrupoles are found to correspond weakly to those of small (spatially locked) three-dimensional disturbances present in the incoming laminar boundary layers. Clearly, the effect of curvature is to affect the rate of decay of the mean streamwise vorticity, at least on the unstable side. The decay of streamwise vorticity is reduced significantly on the unstable side while that on the stable side decays at approximately the same rate as that in the straight wake. Therefore, in the far wake, only a single row of streamwise vortices persisted on the unstable side of the curved case. A very similar effect of destabilizing curvature on the mean streamwise vorticity decay was also observed recently in studies of curved mixing layers (Plesniak *et al.* 1994).

For the tripped cases, spatially stationary streamwise vorticity was not indicated in either the straight or curved wake measurements, thus confirming the sensitivity of the wake structure to initial conditions. Consequently, the tripped cases appear more two-dimensional in the mean. At least for the straight tripped wake, recent direct numerical simulation results show that even temporally variant streamwise vorticity is not generated (Rogers & Moser 1993*b*; Moser & Rogers 1994), in contrast to the early

development of the simulated turbulent mixing layer (Rogers & Moser 1994). The straight tripped case displays a self-similar behaviour, with its defect and half-width obeying the half-power laws and the turbulence profiles plotted in similarity coordinates exhibiting adequate collapse in the far-field region.

The effects of very mild streamwise curvature [$(b/\bar{R})_{max} < 2\%$] are most apparent in the Reynolds stress measurements. The distributions of the Reynolds normal stresses and the primary shear stress are influenced by streamwise curvature such that an asymmetry in levels on the two sides of the wake is developed. The effect of destabilizing curvature is to enhance the stress levels, while that of stabilizing curvature is to decrease them, relative to those in the straight wake. Some, but not all, of the effects of streamwise curvature on the Reynolds stresses can be explained by examining the additional production terms in the transport equations which are activated by the angular momentum instability. The wake half-width is also affected by streamwise curvature. In the near-field, destabilizing curvature increases the growth rate on the unstable side of the wake while stabilizing curvature decreases the growth rate on the stable side of the wake. The very mild curvature of the present investigation does not affect the defect decay rate, in contrast to previous findings for stronger curvature ratios (Ramjee & Neelakandan 1989, 1990).

The present findings have a bearing on a number of practical applications. Mean wake three-dimensionality generated in the initially laminar wake persists a significant distance downstream and thus the performance of many multi-element devices, particularly those operated at relatively low Reynolds numbers (laminar boundary layers), will be affected. The effects of curvature on the wake, even for this case of very mild curvature ($b/\bar{R} < 2\%$), are drastic. The three-dimensional structure of the untripped wake and the streamwise development of both the untripped and tripped wakes are affected significantly by mild streamwise curvature. In most practical applications, such as multi-element airfoils and turbomachinery blades, the wake undergoes a much stronger streamwise curvature. In these cases curvature effects would be even more severe, and perhaps more complex.

This work was supported by and conducted in the Fluid Mechanics Laboratory, NASA Ames Research Center under NASA Grant NCC-2-55 monitored by Dr S. S. Davis. We are grateful to Dr J. H. Bell and Professors L. Roberts, P. Bradshaw and J. P. Johnston for helpful discussions and comments and to Dr R. L. LeBoeuf for reviewing an earlier draft of this paper.

REFERENCES

BELL, J. H. & MEHTA, R. D. 1989 Design and calibration of the mixing layer wind tunnel. *JIAA Rep.* TR-89. Dept. of Aeronautics and Astronautics, Stanford University.

BELL, J. H. & MEHTA, R. D. 1992 Measurements of the streamwise vortical structures in a plane mixing layer. *J. Fluid Mech.* **239**, 213–248.

BELL, J. H., PLESNIAK, M. W. & MEHTA, R. D. 1992 Spanwise averaging of plane mixing layer properties. *AIAA J.* **30**, 835–837.

BRADSHAW, P. 1973 Effects of streamline curvature on turbulent flow. *AGARDograph* 169.

BREIDENTHAL, R. 1980 Response of plane shear layers and wakes to strong three-dimensional disturbances. *Phys. Fluids A* **23**, 1929–1934.

BUELL, J. C. & MANSOUR, N. N. 1989 Near-field structures in three-dimensional spatially-developed wakes. In *Proc. Tenth Australasian Fluid Mechanics Conf., Melbourne, Australia*, pp. 3.21–3.24.

CHEN, J. H., CANTWELL, B. J. & MANSOUR, N. N. 1990 The effect of Mach number on the stability of a plane supersonic wake. *Phys. Fluids* A **2**, 984–1003.

GEORGE, W. K. 1989 The self-preservation of turbulent flows and its relation to initial conditions and coherent structure. In *Advances in Turbulence* (ed. R. Arndt & W. K. George), pp. 75–125. Hemisphere.

GERRARD, J. H. 1966 The three-dimensional structure of the wake of a circular cylinder. *J. Fluid Mech.* **25**, 143–164.

GRANT, H. L. 1958 The large eddies of turbulent motion. *J. Fluid Mech.* **4**, 149–190.

HAYAKAWA, M. & HUSSAIN, F. 1989 Three-dimensionality of organized structures in a plane turbulent wake. *J. Fluid Mech.* **206**, 375–404.

JOVIC, S. & RAMAPRIAN, B. R. 1986 Large-scale structure of the turbulent wake behind a flat plate. *IIHR Rep.* 298. Inst. of Hydraulic Research, University of Iowa.

KOYAMA, H. 1983 Effects of streamline curvature on laminar and turbulent wakes. In *Proc. Fourth Symp. on Turbulent Shear Flows, Karlsruhe, Germany*, pp. 6.32–6.37.

LASHERAS, J. C. & MEIBURG, E. 1990 Three-dimensional vorticity modes in the wake of a flat plate. *Phys. Fluids* A **12**, 371–380.

MAEKAWA, H., MOSER, R. D. & MANSOUR, N. N. 1993 The three-dimensional evolution of a plane wake. In *Proc. Ninth Symp. on Turbulent Shear Flows, Kyoto, Japan, August 16–18*, pp. 3-2-1 to 3-2-6.

MEIBURG, E. & LASHERAS, J. C. 1988 Experimental and numerical investigation of the three-dimensional transition in plane wakes. *J. Fluid Mech.* **190**, 1–37.

MORKOVIN, M. 1964 Flow around circular cylinders- a kaleidoscope of challenging fluid phenomena. *ASME Symp. on Fully Separated Flows*, pp. 102–118.

MOSER, R. D. & ROGERS, M. M. 1994 Direct simulation of a self-similar plane wake. *AGARD Symp. on Application of Direct and Large Eddy Simulation, Crete, Greece*, April 18–21, 1994.

NAKAYAMA, A. 1987 Curvature and pressure-gradient effects on a small-defect wake. *J. Fluid Mech.* **175**, 215–246.

PLESNIAK, M. W., MEHTA, R. D. & JOHNSTON, J. P. 1994 Curved two-stream turbulent mixing layers: three-dimensional structure and streamwise evolution. *J. Fluid Mech.* **270**, 1–50.

POT, P. J. 1979 Measurements in a 2-d wake and in a 2-d wake merging into a boundary layer. *National Aerospace Laboratory Data Report*, NLR TR-79063 U, The Netherlands.

RAMAPRIAN, B. R., PATEL, V. C. & SASTRY, M. S. 1982 The symmetric turbulent wake of a flat plate. *AIAA J.* **20**, 1228–1235.

RAMJEE, V. & NEELAKANDAN, D. 1989 Development of wake of a rectangular cylinder in a curved stream. *Exps Fluids* **7**, 395–399.

RAMJEE, V. & NEELAKANDAN, D. 1990 Curvature effects on the wake of an airfoil and other bodies. *Fluid Dyn. Res.* **6**, 1–13.

RAMJEE, V., TULAPURKARA, E. G. & RAJASEKAR, R. 1988 Development of airfoil wake in a longitudinally curved stream. *AIAA J.* **26**, 948–953.

ROGERS, M. M. & MOSER, R. D. 1992 The three-dimensional evolution of a plane mixing layer: the Kelvin–Helmholtz rollup. *J. Fluid Mech.* **243**, 183–226.

ROGERS, M. M. & MOSER, R. D. 1993*a* Spanwise scale selection in plane mixing layers. *J. Fluid Mech.* **247**, 321–337.

ROGERS, M. M. & MOSER, R. D. 1993*b* The evolution of a self-similar turbulent plane wake. *Bull. Am. Phys. Soc.* **38**, 2271.

ROGERS, M. M. & MOSER, R. D. 1994 Direct simulation of a self-similar turbulent mixing layer. *Phys. Fluids* **6**, 903–923.

ROSHKO, A. 1954 On the development of turbulent wakes from vortex streets. *NACA Rep.* 1191.

SAVILL, A. M. 1983 The turbulence structure of a highly curved two-dimensional wake. In *Structure of Complex Turbulent Shear Flow* (ed. R. Dumas & L. Fulachier). Springer.

TANEDA, S. 1959 Downstream development of the wakes behind cylinders. *J. Phys. Soc. Japan* **14**, 843–848.

TOWSEND, A. A. 1956 *Structure of Turbulent Shear Flow* (1st Edn). Cambridge University Press.

TOWNSEND, A. A. 1976 *Structure of Turbulent Shear Flow* (2nd Edn). Cambridge University Press.

WEI, T. & SMITH, C. R. 1986 Secondary vortices in the wake of circular cylinders. *J. Fluid Mech.* **169**, 513–533.

WEYGANDT, J. H. & MEHTA, R. D. 1993 Three-dimensional structure of straight and curved plane wakes. *JIAA Rep.* TR-110. Dept. of Aeronautics and Astronautics, Stanford University.

WILLIAMSON, C. H. K. 1992 The natural and forced formation of spot-like 'vortex dislocations' in the transition of a wake. *J. Fluid Mech.* **243**, 393–441.

WYGNANSKI, I., CHAMPAGNE, F. & MARASLI, B. 1986 On the large-scale structures in two-dimensional, small-deficit, turbulent wakes. *J. Fluid Mech.* **168**, 31–71.